Accepted Manuscript

Novel resveratrol-based flavonol derivatives: Synthesis and anti-inflammatory activity *in vitro* and *in vivo*

Liu Zeng Chen, Li Yao, Ming Ming Jiao, Jing Bo Shi, Yue Tan, Ban Feng Ruan, Xin Hua Liu

PII: S0223-5234(19)30407-6

DOI: https://doi.org/10.1016/j.ejmech.2019.05.004

Reference: EJMECH 11314

To appear in: *European Journal of Medicinal Chemistry*

Received Date: 18 January 2019

Revised Date: 30 April 2019

Accepted Date: 2 May 2019

Please cite this article as: L.Z. Chen, L. Yao, M.M. Jiao, J.B. Shi, Y. Tan, B.F. Ruan, X.H. Liu, Novel resveratrol-based flavonol derivatives: Synthesis and anti-inflammatory activity *in vitro* and *in vivo*, *European Journal of Medicinal Chemistry* (2019), doi: https://doi.org/10.1016/j.ejmech.2019.05.004.

Graphical abstract

Novel resveratrol-based flavonol derivatives: synthesis and anti-inflammatory activity *in vitro* and *in vivo*

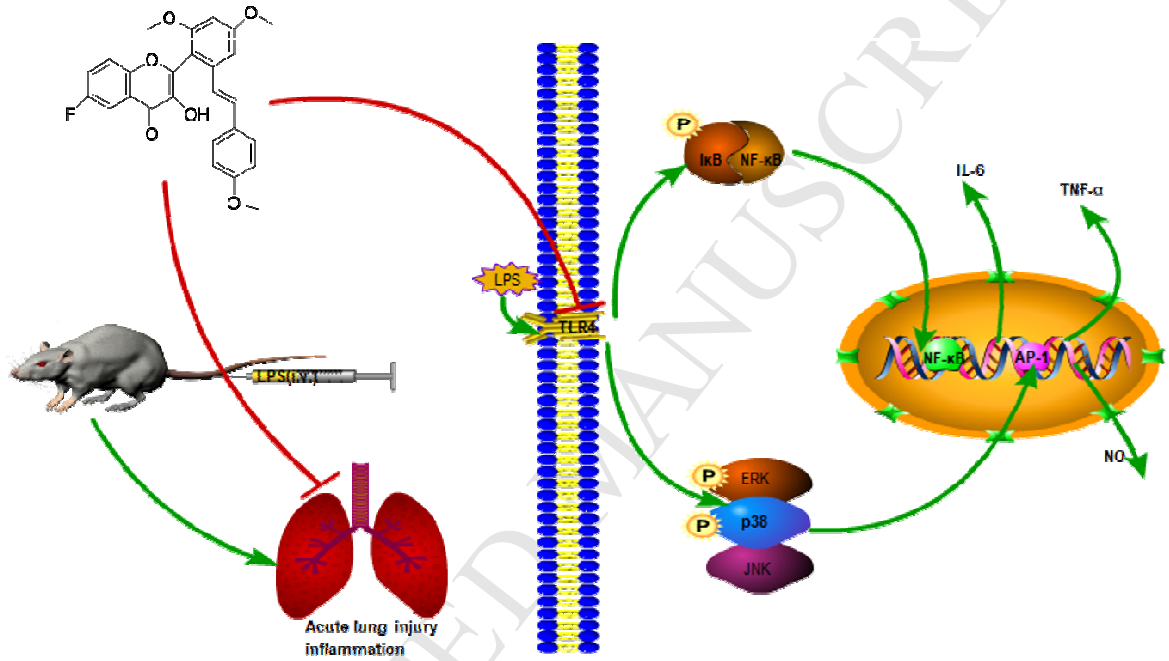

New resveratrol-based flavonol derivatives with anti-inflammatory were synthesized. Among them, one compound could significantly decreased production of NO, IL-6 and TNF-α LPS-stimulated. Preliminary mechanism indicated that it could inhibit expression of TLR4, resulting in activation cell signaling pathway NF-κB and MAPK. The *in vivo* anti-inflammatory activity was determined by LPS-induced acute lung injury.

Novel resveratrol-based flavonol derivatives: synthesis and anti-inflammatory activity *in vitro* and *in vivo*

Liu Zeng Chen [a], Li Yao [b], Ming Ming Jiao [a] Jing Bo Shi [a], Yue Tan [a], Ban Feng Ruan [b,*] and Xin Hua Liu [a,*]

[a] *School of Pharmacy, Anhui Province Key Laboratory of Major Autoimmune Diseases Anhui Medical University, Hefei, 230032, P. R. China*

[b] *School of Food and Biological Engineering, Hefei University of Technology, Hefei, 230009, P. R. China*

Abstract: In order to discover novel anti-inflammatory agents, total thirty-seven new resveratrol-based flavonol derivatives were designed and synthesized. All compounds have been screened for their anti-inflammatory activity by evaluating their inhibition effect of LPS-induced NO production in RAW 264.7 macrophages. Their toxicity was also assessed *in vitro*. Structure-activity relationships (SARs) have been concluded, and finally 2-(2,4-dimethoxy-6-(4-methoxystyryl)phenyl)-3-hydroxy-4H-chromen-4-one was found to be the most active scaffold with low toxicity. This compound could significantly decrease productions of NO, IL-6 and TNF-α with IC_{50} values of 1.35, 1.12 and 1.92 μM, respectively in RAW 264.7 macrophages. Preliminary mechanism studies indicated that it could inhibit the expression of TLR4 protein, resulting in activation of the NF-κB cell signaling pathway. The *in vivo* anti-inflammatory activity of this compound could reduce pulmonary inflammation by mouse model of LPS-induced acute lung injury (ALI). We believe these findings would further support studies of rational design of more efficient acute lung injury regulatory inhibitors.

Keywords: Resveratrol-based flavonol; design; synthesis; anti-inflammatory

*Corresponding author.

Tel.: +86 551 2901438; fax: +86 551 2901438. E-mail addresses: bf_ruan@163.com (Ban Feng Ruan).

Tel.: +86 551 65172353; fax: +86 551 65161115. E-mail addresses: xhliuhx@163.com (Xin Hua Liu).

1. Introduction

Pro-inflammatory cytokines play an important role in the defense of disease [1,2]. however, uncontrolled and excess release of pro-inflammatory mediators such as NO, interleukin-6 (IL-6), interleukin-12 (IL-12), interleukin-1β (IL-1β), tumor necrosis factor alpha (TNF-α) and IL-8 can lead to multiple types of inflammatory diseases such as acute lung injury (ALI) [3-6]. ALI is a critical illness caused by excessive inflammation, with the manifestations of acute respiratory distress, non-cardiogenic pulmonary edema and hypoxemia [7-9]. Many cytokines, such as IL-6, IL-1β and TNF-α have been confirmed to regulate the pathogenesis of ALI through a series of cell cytokine signaling pathways [10,11]. Despite airway management and protective ventilation strategies have been advanced, the mortality rate among ALI patients remains high due to lack of effective drugs [12,13]. Therefore, discovery of highly effective drugs and therapies inhibiting the production and release of pro-inflammatory cytokines for treatment of ALI is urgent.

It has been reported that LPS works by activating its major receptor TLR4, triggering the innate immune systems [14,15], with subsequent activation of nuclear factor (NF-κB) and mitogen-activated protein kinases (MAPK) to induce the release of pro-inflammatory cytokines [16]. Upon stimulation with LPS, TLR4 initiates the series of signaling cascades that result in activation of NF-κB and MAPK to induce the release of pro-inflammatory cytokines such as NO and IL-6 [17].

Resveratrol, a natural product with stilbene moiety which plays an important anti-inflammatory role [18-22], is the most famous lead template for the drug design and discovery [23-25]. In our previous study, based on its good safety profile, diversified derivatives containing resveratrol were designed and synthesized. Among them, resveratrol-based cinnamic ester hybrids indicated good anti-inflammatory activity through reducing proinflammatory cytokines due to its inhibitory effect on the NF-κB signaling pathway. Unfortunately, the activity of these compounds *in vivo* is not satisfactory. We focused on this structure and speculated that the *α*, *β* unsaturated ketone moiety was prone to Michael addition reaction in *vivo*, which should be affect activity (Figure 1). Based on this, we intend to retain the resveratrol skeleton fragments while forming a rigid plane of *α*, *β* unsaturated ketone, and look forward to improving activity. So, as part of our continuous

interest in search of novel resveratrol analogs as anti-inflammatory agents with good bioavailability, other active unit was considered to introduce. As is known, flavonoids in citrus have been widely studied for their potential anti-inflammatory actions, subclasses of dietary flavonoids can alter both bioavailability and bioactivity [26-28]. Therefore, based on these two naturally and pharmaceutically active scaffolds, some new resveratrol-based flavonoid were synthesized (Figure 1), in-house compounds library screening showed that most compounds had no toxicity against tumor cell lines. Further activity tests showed that the toxicity of RAW 264.7 cells was also low. We then evaluated their anti-inflammatory activity *in vitro* and *in vivo*.

Figure 1

2. Results and discussion

2.1 Chemistry

The synthesis of resveratrol aldehyde derivatives (**3a**~**3d**) fragment was exhibited in Scheme 1. Compounds (**2a**~**2d**) were obtained by reacting pterostilbene with a brominated alkane in the presence of potassium carbonate (K_2CO_3) and tetrabutylammonium bromide (TBAB) in acetone under reflux condition. With the Vilsmeier reaction of compounds **2a**~**2d** using $POCl_3$ and DMF afforded the key aldehyde intermediates **3a**~**3d**.

Resveratrol-based flavone derivatives **5a**~**5v** were outlined in Scheme 2. Reaction of resveratrol aldehyde derivatives (**3a**~**3d**) with hydroxyacetophenone derivatives in ethanol in the presence of pyrolidine resulted to compounds **4a**~**4v**. Then, resveratrol chalcone derivatives were treated with iodine (I_2) in DMSO under reflux, compounds **5a**~**5v** were obtained, their structures were shown in Table 1. Resveratrol flavonol derivatives (7**a**~**7o**) were prepared following the procedure described by Scheme 3. The synthesis method of compounds **6a**~**6o** is the same as compounds **4a**~**4v**. Then, resveratrol flavonol derivatives (7**a**~**7o**) were prepared from compounds **6a**~**6o** by treatment with NaOH and 30% H_2O_2 in the presence of methanol at 40 °C. The structures of 7**a**~**7o** shown in Table 2. All compounds were purified by recrystallization or column chromatography and characterized

by ^{1}H NMR, ^{13}C NMR and HRMS (ESI).

Schemes 1~3

Tables 1~2

*2.2 Crystal structure of compounds **5r** and **5u.***

The structure of compound **5r** was determined by X-ray crystallography (Figure 2). Crystallographical data: $C_{30}H_{30}O_6$, Triclinic, space group p_{-1}; a = 9.8786 (7), b = 11.6966(11), c = 22.6393 (17) (Å); α = 93.908 (7), β = 98.968 (6), γ = 94.751 (6) (°), V = 2566.3 (4) nm^3, T =293 (2) K, Z = 4, Dc = 1.259 g/cm^3, $F(000)$ = 1032, Reflections collected/unique =17725/10093, Data/restraints/parameters = 10093/0/657, Goodness of fit on F^2 = 1.073, Fine, R_1 = 0.1167, $wR(F^2)$ = 0.1589. Compound **5u**: $C_{33}H_{28}O_6$, Triclinic, space group p_{-1}; a = 10.1966 (13), b = 16.739 (3), c = 17.174(3) (Å); α = 65.938 (16), β = 76.808 (14), γ = 88.373(12) (°), V = 2599.0(7) nm^3, T = 293(2) K, Z = 4, Dc = 1.33 g/cm^3, $F(000)$ = 1096, Reflections collected/unique = 17809/10212, Data/restraints/parameters = 10212/0/709, Goodness of fit on F^2 = 1.025, Fine, R_1 = 0.1646, $wR(F^2)$ = 0.23. Crystallographic data (excluding structure factors) for the structures have been deposited into the Cambridge Crystallographic Data Center.

(Figure 2)

2.3 Inhibitory activities against LPS-induced NO release

NO is an important pro-inflammatory mediator [29]. Excessive production of NO was found play an important role in many inflammatory diseases [30]. So NO inhibitors accepted that may offer potential opportunity to cure inflammatory diseases [31,32]. RAW 264.7 cells as useful cell model in screening anti-inflammatory drugs, since their stimulation by LPS induces and secretion of pro-inflammatory cytokines such as NO, IL-6 and TNF-α. In order to evaluate the anti-inflammatory activity of synthetic compounds, RAW 264.7 cells were pre-incubated with all compounds (10 μM) for 1 h and treated with

LPS (0.5 μg/mL) for 24 h. The cell conditioned medium was collected, the NO in the media was detected by Griess Reagent assay. The screening results indicated that most of the synthetic compounds could reduce the LPS-induced NO secretion at 10 μM (Figure 3). Among them, compounds **5e** and **5h** showed moderate inhibition of NO compared to that of the positive control Celecoxib. It is noteworthy that compounds **7d**, **7f**, **7i**, **7k** and **7m** exhibited stronger inhibition of NO production compared with the referece compounds celecoxib and resveratrol. According to this, SARs can be easily concluded that introduction of the hydroxyl group to flavonoid is beneficial to NO release activity.

Figure 3

2.4 Assessment of toxicity

Preliminary screening results showed that some compounds had good anti-inflammatory activity. To confirm the need for further evaluation, we then evaluated the cytotoxicity of selected compounds using the MTT assay on the RAW264.7 cell. As showned in Figure 4, most of the compounds shown low toxicity at 20 μM. Compounds **5f**, **5o**, **5u**, **5v**, **7b** and **7n** show weak cytotoxicity. Therefore, these compounds are valuable for further evaluation.

Figure 4

2.5 Inhibition of cytokine production by the active compounds

Two important cytokines, IL-6 and TNF-α have been shown to exert regulating effects on the pathogenesis of ALI through a series of cytokine signaling pathways [33,34]. So, compounds with good NO activity were further tested for inhibition of others inflammatory factors as IL-6 and TNF-α. Cells were pretreated with different concentrations of compounds. The results indicated that most compounds had good IL-6 and TNF-α activity. Among them, compounds **7d**, **7f** and **7i** were selected for further assessment of their concentration dependent inhibitory effects against LPS-induced NO, TNF-α, IL-6 release. Macrophages were pretreated with compounds **7d**, **7f** and **7i**, in a series of concentrations

(10, 5, 2.5, 1.25 and 0.625 μM) for 1 h and with LPS (0.5 μg/ mL) for 24 h. As shown in Figure 5, these compounds significantly decreased NO (IC_{50s} 1.78, 1.35 and 4.83 μM, respectively), IL-6 (IC_{50s} 2.37, 1.12 and 5.06 μM, respectively) and TNF-α (IC_{50s} 5.00, 1.92 and 7.34 μM, respectively) secretion in a concentration-dependent manner. Based on above, compound **7f** is the most prominent one. Thus, compound **7f** was used as the title compound for next mechanism exploration.

Figure 5

2.6 Mechanism explorations of anti-inflammatory activity

2.6.1 Suppression of LPS-induced inflammatory response

NO, being an important signaling molecule, which is also importantly related to modulation expression of iNOS and COX-2 [35]. Activation of cellular pathways leads to high expression of iNOS and COX-2 protein. Thus, inhibitory effects of compound **7f** on LPS-mediated expressions of iNOS and COX-2 were analyzed by Western blot. As shown in Figure 6, the LPS (0.5 μg/mL) stimulation for 24 h could be markedly augmented iNOS and COX-2 expression. However, compound **7f** concentration dependently suppressed LPS-induced iNOS and COX-2 expression. This results once more demonstrated that compound **7f** prevented LPS-induced inflammatory response in macrophages.

Figure 6

2.6.2 Inhibition of LPS-induced ERK and P38 signaling activation

Protein TLR4 is a key protein of the LPS-activated cellular signaling pathway and has been reported as critical for the inflammatory response to LPS [30]. When LPS stimulate cell, TLR4 initiates series of signaling cascades that result in the activation cell signaling pathway including NF-κB and MAPK to induce expression pro-inflammatory proteins [14,31]. Recent studies found that inhibition of TLR4 expression could decrease the expressions of NO, IL-6, TNF-α and IL-1β. So we investigated whether compound **7f** inhibited the expression of TLR4 by Western blot. The results confirmed that TLR4

expression was up-regulated in LPS-induced RAW264.7 cells, which was reversed in a concentration-dependent manner by pretreated with compound **7f**.

NF-κB and MAPKs are also known to participate in regulating the inflammatory process. MAPK, including ERK, p38, and JNK were quite significant in the regulation of inflammation [35,36]. LPS-stimulated macrophages can activate MAPKs signaling path, allowing the transcription factors AP-1 translocate into the nucleus and bind to target promoters turn on transcriptions of inflammatory genes including production of NO, TNF-α, IL-6 and other inflammatory mediators [30]. Therefore, we detected the effects of compound **7f** on LPS-mediated MAPK signaling activation by Western blot. Consistent with previous reports of LPS time dependently activation MAPK (JNK, p38 and ERK) and caused a peak level of phospho-rylated MAPK (JNK2, p38 and ERK) at 15 or 30 min in RAW264.7 cells. Interestingly, compound **7f** only concentration-dependent blocked LPS-induced ERK phosphorylation and p38 phosphorylation, but not JNK phosphorylation. Moreover, total protein levels of ERK, JNK and P38 were not affected by LPS and treatment of compound **7f** (Figure 7).

Figure 7

2.6.3 Inhibition of activation of LPS-induced NF-kB signaling pathway

NF-κB is one of the principal factors for the production proinflammatory cytokines associated with LPS-induced signaling pathways [36]. Among NF-κB family, the transcription factor P65 plays the most important role in the development of inflammation [37-38]. A large number of inflammation cytokines stimuli such as LPS, TNF-α and IL-1β can activation of IκB kinase (IKK), which in turn phosphorylates IκB. Phosphorylates IκB results in its ubiquitination and degradation by the proteasome, allowing the liberated NF-κB to translocate into the nucleus and bind to target promoters turn on transcriptions of inflammatory genes. Herein, we analyzed them by Western blot. The results showed compound **7f** could be effect of IκB proteins phosphorylation and degradation (Figure 8). Meanwhile, it maybe inhibits NF-κB p65 translocate into the nucleus.

Figure 8

2.7 Molecular docking

It has been reported that Tak1 is traditionally accepted as the primary LPS receptor and critical for the inflammatory response to LPS [14-17]. Upon stimulation with LPS, TLR4 initiates series of signaling cascades that result in activation of TAK1 signal pathway. Tak1 could activate NF-κB and MAPK, then induce the release of pro-inflammatory cytokines.

In order to elucidate the mechanism by which compound **7f** can induce the release of pro-inflammatory cytokine. Molecular docking of this compound into binding site of human TAK1 was performed (Discovery Studio 2018). The result shows that compound **7f** may well bind to TAK1 and can form interaction with Val42, Val50, Cys174, Leu163. Its 4-position carbonyl forms a stable hydrogen bond interaction with Tyr106. These results suggested that the anti-inflammatory activity of compound **7f** might be bind to TAK1 protein **(**Figure 9**)**.

Figure 9

*2.8 In vivo activity of compound **7f***

To evaluate the activity *in vivo*, compound **7f** was next evaluated with the ALI rat model. C57/BL6 mice were treated by intraperitoneal injection with compound **7f** (15 mg/kg), and after 30 min, were challenged with 5 mg/kg LPS by intratracheal injection. Myeloperoxidase (MPO) is released from the cytoplasmic granules of activated phagocytes, and as such, measurement of MPO activity in whole lung homogenates reflects the accumulation of neutrophils in the lungs. As showned in Figure 10A, LPS significantly increased MPO activity of lung tissue compared to the control group, in which the administration of compound **7f** effectively prevented the increase. Besides, due to LPS challenge significantly reduce body weight, however, compound **7f** seemed to have little effect on the weight loss induced by LPS. Lung wet/dry weight ratio was calculated to assess pulmonary edema. LPS significantly increased the lung Wet/Dry ratio (W/D). However, compound **7f** was able to reduce or prevent lung injury in ALI mice (Figure 10B). In addition, to further research the protective effect of compound **7f** against LPS-induced ALI. As depicted in Figure 10C, with the challenge of LPS, the survival rate

of ALI mice at 24 h was 60% while administration of compound **7f** improved the survival rate of 90%. When LPS challenge was extended to 48 h, most mice dead. Compound **7f** (20 mg/kg) could markedly increase the survival rate of ALI mice from 10% to 50% (Figure 10D). To assess histological changes in LPS-challenged mice following treatment with compound **7f**, we performed hematoxylin and eosin (H&E) staining (Figure 10E). LPS instillation led to significant pro-inflammatory alterations, alveolar hemorrhage, including lung edema, inflammatory cell infiltration, and destruction of alveolar structure. These histopathological changes were improved with treatment of either 10 and 20 mg/kg of compound **7f**. These studies showed that compound **7f** had a protective effect on LPS-induced histopathological changes in a mouse model of ALI.

In order to determine what is the toxicity profile of the most active compound **7f** on experimental animals, mice were treated with compound **7f** (20 mg/kg) solutions by intraperitoneal injection. The mice live normally, no differences compared to the control group. lung sections were subjected to hematoxylin and eosin staining. we couldn't find significant pro-inflammatory alterations, alveolar hemorrhage, including lung edema, inflammatory cell infiltration, and destruction of alveolar structure. Lung tissues showed a normal structure and no histopathological change under a light microscope (Figure 11).

Figures 10~11

3. Conclusions

In summary, based on finding novel compounds with activity of acute lung injury, thirty-nine resveratrol-based flavonol derivatives were designed and synthesized. The initial evaluation results showed that most compounds had good NO inhibitory activity and low toxicity. According to SARs, the introduction of a hydroxyl group into flavonoid is beneficial to anti-inflammatory activity. Specifically, the title compound **7f** could inhibit IL-6, NO and TNF-α secretion in a dose-dependent manner. The preliminary mechanism indicated that this compound suppressed LPS-induced expressions of iNOS and COX-2, and productions of IL-6, TNF-α and NO through NF-κB/MAPK signaling pathway in a concentration dependent manner (Figure 12). The further study *in vivo* showed that the title

compound **7f** effectively reduced LPS-induced pulmonary inflammation and acute lung injury in mouse model. Compared to resveratrol-based cinnamic ester hybrids (our previous work) and the title compounds synthesized in this resveratrol-based flavonols (this work), the anti-inflammatory activity of the title compound was dramatically enhanced at the cellular level, and the activity of acute lung injury was further confirmed by animal experiments *in vivo*. In addition, the toxicity of these compounds is lower than previous compounds [22].

Figure 12

4. Experimental section

4.1 Chemistry

In general, all reagents used in the synthesis were obtained from Aladdin. Adamas, Tan soole *et al*. without further purifications. Reactions were monitored by analytical thin-layer chromatography (TLC) and visualized under UV light (λ=254 or 365 nm). Purification by chromatography column were carried on using silica gel (200-300 meshes). Fourier transform mid-infrared spectra were measured using a Nicolet 6700 spectrometer (Thermo Fisher Scientific Inc., Madison, WI) with SMART iTR attenuated total reflectance (ATR) accessory. All the ^{1}H and ^{13}C NMR (Nuclear Magnetic Resonance) spectra were recorded either with a Agilent 400 or 600 MHz spectrometer. The ESI-MS spectra were recorded on a Mariner System 5304 Mass spectrometer. Melting points were determined on a XT4MP apparatus (Taike Corp., Beijing, China), and uncorrected.

4.2 Crystallographic studies

Compounds **5r** and **5u** were chosen for X-ray diffraction analysis performed on a BRUCKER SMART APEX-CCD diffractometer equipped with a graphite monochromatic MoKa radiation (λ = 0.71073 A) radiation at 293(2) K. A total reflections were collected in the range of $0.97<\theta<26.1^{o}$ by using a ψ-ω scan mode with independent ones, of which $I>2\sigma(I)$ were observed and used in the succeeding refinements. The data set were corrected

by SADABS program and the structure were solved by direct methods with SHELXS-97 and refined by full-matrix least-squares method on F^2 with SHELXL-97 [39]. The non-hydrogen atoms were refined anisotropically, and the hydrogen atoms were added according to theoretical models. The structures were refined by full-matrix least-squares method on F^2 with SHELXT-97.

4.3 Synthesis of resveratrol-based flavone derivatives **5a**~**5v**

A solution containing of compounds ***4a***~***4v*** (1 mmol, 1.0 equiv) and I_2 (0.01 mmol, 0.01 equiv) in dimethyl sulfoxide (15 mL) was stirred for 4-6 h at 130 °C. Then the resulting mixture was slowly added to a solution of ice-water, stirred for 2 h and filtered to obtain the crude product. Which was purified by column chromatography on silica gel (EtOAc/petroleum ether = 1:3), to afford the corresponding pure products ***5a***~***5v*** (Scheme 1). The final products provided the following data.

(E)-2-(2,4-dimethoxy-6-(4-methoxystyryl)phenyl)-4H-chromen-4-one (***5a***). White solid, Yield: 90%, Mp: 193-197 °C. ^{1}H NMR (600MHz, $CDCl_3$) δ 8.27 (d, *J* = 7.8 Hz, 1H), 7.65 (t, *J* = 7.7 Hz, 1H), 7.43 (dd, *J* = 14.9, 7.8 Hz, 2H), 7.28 (d, *J* = 8.5 Hz, 2H), 7.07-6.98 (m, 1H), 6.92-6.83 (m, 2H), 6.80 (d, *J* = 8.6 Hz, 2H), 6.44 (d, *J* = 21.6 Hz, 2H), 3.92 (s, 3H), 3.78 (t, *J* = 5.8 Hz, 6H). ^{13}C NMR (151 MHz, $CDCl_3$): δ 173.36 (s), 163.97 (s), 162.31 (s), 160.96 (s), 157.47 (s), 146.85 (s), 142.56 (s), 141.89 (s), 135.75 (s), 133.61 (s), 132.11 (s), 130.51 (s), 127.14 (s), 127.04 (s), 124.85 (s), 128.08 (s), 120.15 (s), 115.78 (s), 113.98 (s), 103.94 (s), 100.63 (s), 57.61 (s), 57.46 (s), 56.89 (s). MS (ESI): 415.1440. MS(ESI): 415.1440 ($C_{26}H_{23}O_5$, $[M+H]^+$).

(E)-2-(2,4-dimethoxy-6-(4-methoxystyryl)phenyl)-7-methyl-4H-chromen-4-one (***5b***). White solid, Yield: 61%, Mp: 186-189 °C. ^{1}H NMR (600 MHz, DMSO) δ 7.95 (d, *J* = 8.1 Hz, 1H), 7.41 (s, 1H), 7.35 (d, *J* = 8.7 Hz, 2H), 7.31 (d, *J* = 8.1 Hz,1H), 7.25 (d, *J* = 16.1 Hz, 1H), 7.01 (t, *J* = 4.2 Hz, 1H), 6.87-6.83 (m, 3H), 6.62 (d, *J* =1.9 Hz, 1H), 6.23 (s, 1H), 3.88 (s, 3H), 3.75 (s, 3H), 3.69 (d, *J* = 3.7 Hz, 3H), 2.42 (s,3H). ^{13}C NMR (101 MHz, $CDCl_3$): δ 175.27 (s), 162.78 (s), 160.29 (s), 159.73 (s),156.29 (s), 147.14 (s), 145.65 (s), 142.22 (s),

139.47 (s), 131.87 (s), 130.13 (s), 128.89(s), 126.93 (s), 124.89(s), 123.64 (s), 120.73 (s), 118.87 (s), 99.87(s), 98.79 (s), 113.18(s), 110.76 (s), 56.85 (s), 55.81 (s), 55.95 (s), 20.95 (s). MS(ESI): 429.1697 ($C_{27}H_{25}O_5$, $[M+H]^+$).

(E)-2-(2,4-dimethoxy-6-(4-methoxystyryl)phenyl)-6-methyl-4H-chromen-4-one (***5c***). White solid, Yield: 59%, Mp: 187-192 °C. ^{1}H NMR (600 MHz, $CDCl_3$) δ 8.07(s, 1H), 7.46 (d, *J* = 8.0 Hz, 1H), 7.34 (d, *J* = 8.5 Hz, 1H), 7.28 (d, *J* = 8.5 Hz, 2H), 7.03 (d, *J* = 16.0 Hz, 1H), 6.92-6.84 (m, 2H), 6.80 (d, *J* = 8.5 Hz, 2H), 6.44 (d, *J* = 29.6 Hz, 2H), 3.92 (s, 3H), 3.78 (d, *J* = 1.7 Hz, 6H), 2.48 (s, 3H). ^{13}C NMR (101 MHz, $CDCl_3$): δ 168.94(s), 161.46 (s), 158.79 (s), 156.89 (s), 154.56 (s), 143.94 (s), 136.73 (s), 135.54 (s), 134.79 (s), 134.12 (s), 130.98 (s), 128.93 (s), 128.14 (s), 125.17 (s), 122.81 (s), 120.91 (s), 117.94 (s), 113.89 (s), 110.95 (s), 100.96 (s), 98.80 (s), 58.03 (s), 54.73 (s), 52.43 (s), 22.98 (s). MS(ESI): 429.1694 ($C_{27}H_{25}O_5$, $[M+H]^+$).

(E)-2-(2,4-dimethoxy-6-(4-methoxystyryl)phenyl)-6,7-dimethyl-4H-chromen-4-one (***5d***). White solid, Yield: 72%, Mp: 203-207 °C. IR (ATR Diamond Crystal, cm^{-1}): *v* 2972, 1620, 1596, 1461, 1332, 1302, 1159, 1177, 967, 830; ^{1}H NMR (600 MHz, $CDCl_3$) δ 7.98 (d, *J* = 35.8 Hz, 1H), 7.28 (d, *J* = 8.5 Hz, 2H), 7.22 (s, 1H), 7.03 (d, *J* =16.0 Hz, 1H), 6.91-6.84 (m, 2H), 6.80 (d, *J* = 8.5 Hz, 2H), 6.46 (s, 1H), 6.38 (s, 1H), 3.92 (s, 3H), 3.77 (s, 6H), 2.37 (d, *J* = 9.2 Hz, 5H). ^{13}C NMR (101 MHz, $CDCl_3$): δ 179.68 (s), 163.59 (s), 158.97 (s), 157.81 (s), 156.16 (s), 145.27 (s), 145.00 (s), 138.98 (s), 137.50 (s), 135.64 (s), 130.29 (s), 128.97 (s), 128.15 (s), 123.83 (s), 122.66 (s), 109.98 (s), 107.67 (s), 106.88 (s), 103.62 (s), 101.30 (s), 99.00 (s), 57.02 (s), 56.54 (s), 56.19 (s), 21.65 (s), 20.19 (s). MS(ESI): 443.1854 ($C_{28}H_{27}O_5$, $[M+H]^+$).

(E)-2-(2,4-dimethoxy-6-(4-methoxystyryl)phenyl)-6-methoxy-4H-chromen-4-one (***5e***). Yellow solid, Yield: 66%, Mp: 168-170 °C. ^{1}H NMR(600 MHz, $CDCl_3$) δ 7.64 (d, *J* = 2.9 Hz, 1H), 7.39 (d, *J* = 9.1 Hz, 1H), 7.28 (d, *J* = 8.6 Hz, 2H), 7.26-7.24 (m, 1H), 7.03 (d, *J* = 16.0 Hz, 1H), 6.87 (d, *J* = 15.9 Hz, 2H), 6.80 (d, *J* = 8.6 Hz, 2H), 6.44 (d, *J* = 22.9 Hz, 2H), 3.92 (s, 6H), 3.78 (s, 6H). ^{13}C NMR (101 MHz, DMSO): δ 178.09 (s), 164.72 (s), 161.29

(s), 159.73 (s), 156.44 (s), 149.82 (s), 146.91 (s), 141.76 (s), 140.53 (s), 131.79 (s), 129.02 (s), 125.83 (s), 122.48 (s), 120.70 (s), 117.63 (s), 115.05 (s), 114.28 (s), 112.05 (s), 100.96 (s), 98.92 (s), 96.80 (s), 57.86 (s), 55.09 (s), 53.51 (s), 45.05 (s). MS(ESI): 445.1650 ($C_{27}H_{25}O_6$, $[M+H]^+$).

(E)-2-(2,4-dimethoxy-6-(4-methoxystyryl)phenyl)-6,7-dimethoxy-4H-chromen-4-one (***5f***). Yellow solid, Yield: 42%, Mp: 188-192 °C. ^{1}H NMR (600 MHz, DMSO) δ 7.39 (s, 1H), 7.33 (d, *J* = 8.7 Hz, 2H), 7.25 (d, *J* = 16.2 Hz, 1H), 7.20 (s, 1H), 7.00 (d, *J* = 1.8 Hz, 1H), 6.85 (t, *J* = 11.6 Hz, 2H), 6.81 (d, *J* = 16.2 Hz, 1H), 6.61 (t, *J* = 3.0 Hz, 1H), 6.19 (s, 1H), 3.88 (s, 3H), 3.86 (s, 3H), 3.84 (s, 3H), 3.75 (s, 3H), 3.70 (s, 3H). ^{13}C NMR (101 MHz, DMSO): δ 178.09 (s), 164.72 (s), 161.29 (s), 159.73 (s), 156.44 (s), 149.82 (s), 146.91 (s), 141.76 (s), 140.53 (s), 131.79 (s), 129.02(s), 125.83 (s), 122.48 (s), 120.70 (s), 117.63 (s), 115.05 (s), 114.28 (s), 112.05 (s), 100.96 (s), 98.92 (s), 96.80 (s), 57.86 (s), 55.09 (s), 53.51 (s), 42.05(s), 39.67 (s). MS(ESI): 475.1760 ($C_{28}H_{27}O_7$, $[M+H]^+$).

(E)-2-(2,4-dimethoxy-6-(4-methoxystyryl)phenyl)-7-fluoro-4H-chromen-4-one (***5g***). Yellow solid, Yield: 78%, Mp: 186-191 °C. ^{1}H NMR (600 MHz, $CDCl_3$) δ 8.28 (dd, *J* = 8.5, 6.5 Hz, 1H), 7.29 (d, *J* = 8.5 Hz, 2H), 7.14 (dd, *J* = 20.3, 8.8 Hz, 2H), 7.03 (d, *J* = 16.0 Hz, 1H), 6.89-6.78 (m, 4H), 6.49-6.39 (m, 2H), 3.93 (s, 3H), 3.79 (d, *J* = 1.1 Hz, 6H). ^{13}C NMR (101 MHz, DMSO): δ 185.91 (s), 174.63 (s), 165.87 (s), 155.84 (s), 150.16 (s), 147.85 (s), 145.32 (s), 139.04 (s), 137.53 (s), 129.72 (s), 127.91 (s), 125.95 (s), 123.96 (s), 123.56 (s), 120.94 (s), 118.90 (s), 115.64 (s), 113.64 (s), 108.12 (s), 102.95 (s), 98.70 (s), 53.88 (s), 50.52 (s), 45.65 (s). MS(ESI): 433.1449 ($C_{26}H_{22}FO_5$, $[M+H]^+$).

(E)-2-(2,4-dimethoxy-6-(4-methoxystyryl)phenyl)-6-fluoro-4H-chromen-4-one (***5h***). White solid, Yield: 59%, Mp: 216-220 °C. IR (ATR Diamond Crystal, cm^{-1}): *v* 3002, 2936, 2836, 1640, 1568, 1474, 1340, 1240, 1085, 843; ^{1}H NMR (600 MHz, $CDCl_3$) δ 7.91 (dd, *J* = 8.1, 2.4 Hz, 1H), 7.45 (dd, *J* = 9.0, 3.9 Hz, 1H), 7.38 (dd, *J* = 11.4, 5.1 Hz, 1H), 7.28 (d, *J* = 8.5 Hz, 2H), 7.03 (d, *J* = 16.0 Hz, 1H), 6.91-6.79 (m, 4H), 6.45 (d, *J* = 25.2 Hz, 2H), 3.93 (s, 3H), 3.79 (d, *J* = 2.5 Hz, 6H). ^{13}C NMR (101 MHz, DMSO): δ 171.91 (s), 161.93 (s),

159.20 (s), 158.84 (s), 157.16 (s), 151.85 (s), 146.32 (s), 140.04 (s), 138.63 (s), 130.92 (s), 129.21 (s), 127.95 (s), 123.16 (s), 122.56 (s), 121.74 (s), 121.20 (s), 114.14 (s), 111.44 (s), 109.12 (s), 100.95 (s), 97.78 (s), 55.88 (s), 55.52 (s), 55.05 (s). MS(ESI): 433.1441 ($C_{26}H_{22}FO_5$, $[M+H]^+$).

(E)-8-chloro-2-(2,4-dimethoxy-6-(4-methoxystyryl)phenyl)-4H-chromen-4-one (***5i***). White solid, Yield: 58%, Mp: 231-234 °C. ^{1}H NMR (400 MHz, $CDCl_3$) δ 8.29 (d, *J* = 7.9 Hz, 1H), 7.66 (t, *J* = 7.7 Hz, 1H), 7.47-7.40 (m, 2H), 7.31-7.24 (m, 2H), 6.88 (dd, *J* = 14.6, 8.7 Hz, 2H), 6.81 (d, *J* = 8.4 Hz, 2H), 6.47 (s, 2H), 3.93 (s, 3H), 3.78 (d, *J* = 4.7 Hz, 6H). ^{13}C NMR (101 MHz, DMSO): δ 182.91 (s), 167.63 (s), 160.16 (s), 159.864 (s), 158.06 (s), 152.75 (s), 148.02 (s), 141.24 (s), 139.53 (s), 131.52 (s), 128.91 (s), 128.05 (s), 122.16 (s), 121.56 (s), 120.74 (s), 120.20 (s), 115.14 (s), 112.14 (s), 108.62 (s), 100.35 (s), 96.78 (s), 57.12 (s), 54.82 (s), 52.05 (s). MS(ESI): 449.1147 ($C_{26}H_{22}ClO_5$, $[M+Na]^+$).

(E)-7-chloro-2-(2,4-dimethoxy-6-(4-methoxystyryl)phenyl)-4H-chromen-4-one (***5j***). White solid, Yield: 68%, Mp: 221-225 °C. ^{1}H NMR(400 MHz, $CDCl_3$) δ 8.17 (d, *J* = 8.4 Hz, 1H), 7.29 (d, *J* = 8.5 Hz, 2H), 7.25 (s, 1H), 7.04 (d, *J* = 16.1 Hz, 1H), 6.89 (d, *J* = 18.3 Hz, 2H), 6.81 (d, *J* = 8.4 Hz, 2H), 6.46 (s, 2H), 3.93 (s, 3H), 3.79 (s, 6H). ^{13}C NMR (101 MHz, $CDCl_3$): δ 187.51 (s), 175.63 (s), 168.26 (s), 159.84 (s), 158.16 (s), 156.15 (s), 149.12 (s), 145.14 (s), 140.43 (s), 133.62 (s), 129.91 (s), 128.25 (s), 122.46 (s), 120.86 (s), 119.74 (s), 118.20 (s), 115.64 (s), 112.04 (s), 109.62 (s), 99.35 (s), 95.78 (s), 58.12 (s), 52.82 (s), 50.05 (s). MS(ESI): 471.0970 ($C_{26}H_{22}ClO_5$, $[M+Na]^+$).

(E)-6-chloro-2-(2,4-dimethoxy-6-(4-methoxystyryl)phenyl)-4H-chromen-4-one (***5k***). White solid, Yield: 71%, Mp: 227-229 °C. ^{1}H NMR (400 MHz, $CDCl_3$) δ 8.01 (s, 1H), 7.31-7.25 (m, 2H), 7.03 (d, *J* = 16.1 Hz, 1H), 6.88 (d, *J* = 16.8 Hz, 2H), 6.80 (d, *J* = 8.5 Hz, 2H), 6.45 (d, *J* = 7.3 Hz, 1H), 6.39 (s, 1H), 3.92 (s, 3H), 3.78 (s, 6H). ^{13}C NMR (101 MHz, $CDCl_3$): δ 179.51 (s), 170.73 (s), 168.66 (s), 160.24 (s), 158.56 (s), 154.65 (s), 148.12 (s), 146.34 (s), 137.73 (s), 134.62 (s), 128.93 (s), 127.85 (s), 124.46 (s), 119.86 (s), 113.84 (s), 110.78 (s), 108.64 (s), 100.04 (s), 98.62 (s), 78.35 (s), 74.78 (s), 46.88 (s), 45.82 (s), 41.65 (s). MS(ESI): 471.0970 ($C_{26}H_{21}ClO_5$, $[M+Na]^+$).

(E)-7-bromo-2-(2,4-dimethoxy-6-(4-methoxystyryl)phenyl)-4H-chromen-4-one (***5l***). White solid, Yield: 75%, Mp: 219-220 °C. IR (ATR Diamond Crystal, cm^{-1}): *v* 2988, 2900, 1647, 1595, 1511,1418, 1333, 1080, 963, 829; ^{1}H NMR (600 MHz, $CDCl_3$) δ 8.13 (d, *J* = 8.5 Hz, 1H), 7.64 (s, 1H), 7.54 (d, *J* = 8.5 Hz, 1H), 7.29 (d, *J* = 8.5 Hz, 2H), 7.03 (d, *J* = 16.0 Hz, 1H), 6.87-6.80 (m, 3H), 6.43 (d, *J* = 31.4 Hz, 2H), 3.93 (s, 3H), 3.79 (s, 6H). ^{13}C NMR (101 MHz, $CDCl_3$): δ 181.51 (s), 172.87 (s), 169.16 (s), 161.34 (s), 159.46 (s), 154.35 (s), 150.32 (s), 147.64 (s), 134.73 (s), 130.12 (s), 128.23 (s), 126.55 (s), 124.36 (s), 118.86 (s), 113.54 (s), 111.78 (s), 109.74 (s), 101.02 (s), 99.32 (s), 86.35 (s), 79.28 (s), 56.88 (s), 55.12 (s), 40.25 (s). MS(ESI): 515.0465 ($C_{26}H_{21}BrO_5Na$, $[M+Na]^+$).

(E)-6-bromo-2-(2,4-dimethoxy-6-(4-methoxystyryl)phenyl)-4H-chromen-4-one (***5m***). White solid, Yield: 88%, Mp: 225-229 °C. ^{1}H NMR (600 MHz, DMSO) δ 8.14 (d, *J* = 2.1 Hz, 1H), 7.93 (dd, *J* = 8.9, 2.2 Hz, 1H), 7.61 (d, *J* = 8.9 Hz, 1H), 7.39 (d, *J* = 8.6 Hz, 2H), 7.25 (d, *J* = 16.1 Hz, 1H), 7.01 (s, 1H), 6.91-6.86 (m, 1H), 6.85 (d, *J* = 8.6 Hz, 2H), 6.62 (s, 1H), 6.34 (s, 1H), 3.89 (s, 3H), 3.75 (s, 3H), 3.70 (s, 3H). ^{13}C NMR (101 MHz, $CDCl_3$): δ 180.51 (s), 176.87 (s), 162.96 (s), 160.34 (s), 158.96 (s), 154.15 (s), 151.32 (s), 148.34 (s), 136.73 (s), 131.12 (s), 129.53 (s), 126.65 (s), 125.16 (s), 119.86 (s), 113.44 (s), 110.78 (s), 106.74 (s), 101.32 (s), 98.32 (s), 85.35 (s), 77.28 (s), 55.84 (s), 53.42 (s), 50.25 (s). MS(ESI): 515.0465 ($C_{26}H_{21}BrO_5Na$, $[M+Na]^+$).

(E)-2-(2-(4-ethoxystyryl)-4,6-dimethoxyphenyl)-4H-chromen-4-one (***5n***). White solid, Yield: 93%, Mp: 178-180 °C. IR (ATR Diamond Crystal, cm^{-1}): *v* 2981, 2901, 1636, 1600, 1566, 1461, 1238, 1178, 1051, 755; ^{1}H NMR (400 MHz, DMSO) δ 8.11 (d, *J* = 7.1 Hz, 1H), 7.81 (t, *J* = 7.7 Hz, 1H), 7.63 (d, *J* = 8.4 Hz, 1H), 7.53 (t, *J* = 7.5 Hz, 1H), 7.37 (d, *J* = 8.6 Hz, 2H), 7.27 (d, *J* = 16.1 Hz, 1H), 7.03 (d, *J* = 1.5 Hz, 1H), 6.87 (dd, *J* = 19.3, 12.4 Hz, 3H), 6.66 (s, 1H), 6.31 (s, 1H), 3.99 (q, *J* = 6.9 Hz, 2H), 3.92 (s, 3H), 3.78 (s, 3H), 1.29 (t, *J* = 6.9 Hz, 3H). ^{13}C NMR (101 MHz, $CDCl_3$): δ 181.53 (s), 174.57 (s), 163.46 (s), 161.24 (s), 159.74 (s), 153.45 (s), 150.46(s), 149.20 (s), 137.93 (s), 130.56 (s), 128.78 (s), 125.93

(s), 123.59 (s), 118.05 (s), 111.97 (s), 109.64 (s), 106.89 (s), 100.98 (s), 96.83 (s), 84.96 (s), 74.95 (s), 54.43 (s), 52.34 (s), 50.29 (s), 42.89(s). MS(ESI): 451.1516 ($C_{27}H_{24}O_5Na$, $[M+Na]^+$).

(E)-2-(2-(4-ethoxystyryl)-4,6-dimethoxyphenyl)-6-methoxy-4H-chromen-4-one (***5o***). White solid, Yield: 83%, Mp: 167-169 °C. IR (ATR Diamond Crystal, cm^{-1}): *v* 2971, 2901, 1639, 1592, 1568, 1486, 1331, 1156, 1074, 1037, 829, 816; ^1H NMR (600 MHz, $CDCl_3$): *δ* 8.03(d, *J* = 3.1 Hz, 1H), 7.86 (s, 1H), 7.55 (s, 1H), 7.31 (d, *J* = 8.2 Hz, 1H), 7.18 (s, 2H), 6.80 (d, *J* = 16.1 Hz, 1H), 6.61 (s, 2H), 6.51 (d, *J* = 16.1 Hz, 1H), 6.34 (s, 1H), 6.21 (s, 1H), 3.53 (d, *J* = 3.2 Hz, 6H), 3.23 (s, 3H), 3.01 (dd, 2H), 1.58 (t, *J* =3.2 Hz, 3H). ^{13}C NMR (101 MHz, $CDCl_3$): δ 180.24 (s), 175.23 (s), 165.85 (s), 161.97 (s), 149.74 (s), 143.45 (s), 139.56(s), 128.97 (s), 126.43 (s), 124.56 (s), 120.78 (s), 118.93 (s), 113.59 (s), 107.05 (s), 102.97 (s), 100.64 (s), 98.89 (s), 86.98 (s), 84.83 (s), 80.96 (s), 67.95 (s), 45.43 (s), 42.34 (s), 40.89 (s), 40.09(s), 35.27(s). MS(ESI): 481.1622 ($C_{28}H_{26}O_6Na$, $[M+Na]^+$).

(E)-6-bromo-2-(2-(4-ethoxystyryl)-4,6-dimethoxyphenyl)-4H-chromen-4-one (***5p***). White solid, Yield: 88%, Mp: 243-244 °C. IR (ATR Diamond Crystal, cm^{-1}): *v* 3017, 2978, 2931, 2882, 1633, 1568, 1428, 1237, 1085, 803; ^1H NMR (400 MHz, DMSO) δ 8.17 (d, *J* = 2.5 Hz, 1H), 7.96 (dd, *J* = 8.9, 2.5 Hz, 1H), 7.63 (d, *J* = 8.9 Hz, 1H), 7.40 (d, *J* = 8.7 Hz, 2H), 7.27 (d, *J* = 16.1 Hz, 1H), 7.03 (d, *J* = 2.0 Hz, 1H), 6.94-6.87 (m, 1H), 6.85 (d, *J* = 8.7 Hz, 2H), 6.65 (d, *J* = 2.0 Hz, 1H), 6.36 (s, 1H), 3.99 (q, *J* = 7.0 Hz, 2H), 3.91 (s, 3H), 3.78 (s, 3H), 1.29 (t, *J* = 7.0 Hz, 3H). ^{13}C NMR (101 MHz, $CDCl_3$) δ 179.64 (s), 175.13 (s), 163.45 (s), 162.97 (s), 152.85 (s), 150.45 (s), 149.43(s), 126.34 (s), 125.83 (s), 123.78 (s), 121.53 (s), 119.53 (s), 115.73 (s), 108.25 (s), 103.52 (s), 101.47 (s), 100.89 (s), 98.25 (s), 91.33 (s), 83.32 (s), 75.95 (s), 52.55 (s), 49.43 (s), 47.16 (s), 39.96(s). MS(ESI): 529.0621 ($C_{27}H_{23}BrO_5Na$, $[M+Na]^+$).

(E)-2-(2-(4-butoxystyryl)-4,6-dimethoxyphenyl)-4H-chromen-4-one (***5q***). Yellow solid, Yield: 89%, Mp: 167-169 °C. IR (ATR Diamond Crystal, cm^{-1}): *v* 2958, 2931, 2871, 1640, 1596, 1574, 1463, 1350, 1248, 1203, 1156, 1075, 829, 748; ^1H NMR (600 MHz, DMSO) δ

8.08 (dd, *J* = 7.9, 1.2 Hz, 1H), 7.78 (t, *J* = 7.8 Hz, 1H), 7.60 (d, *J* = 8.4 Hz, 1H), 7.50 (t, *J* = 7.5 Hz, 1H), 7.34 (d, *J* = 8.6 Hz, 2H), 7.24 (d, *J* = 16.1 Hz, 1H), 7.01 (d, *J* = 1.7 Hz, 1H), 6.89- 6.84 (m, 1H), 6.83 (d, *J* = 8.5 Hz, 2H), 6.62 (d, *J* = 1.6 Hz, 1H), 6.28 (s, 1H), 3.92-3.89 (m, 2H), 3.89 (s, 3H), 3.75 (s, 3H), 1.65-1.59 (m, 2H), 1.40-1.33 (m, 2H), 0.87 (t, *J* = 7.4 Hz, 3H). ^{13}C NMR (101 MHz, $CDCl_3$): δ 181.21 (s), 172.65 (s), 159.27 (s), 149.08 (s), 145.09 (s), 140.47 (s), 139.05 (s), 135.67 (s), 130.28 (s), 129.53 (s), 123.33 (s),120.63 (s), 120.34 (s), 119.38 (s), 116.91 (s), 114.83 (s), 110.74 (s), 100.66 (s), 100.15 (s), 99.85 (s), 97.30 (s), 66.49 (s), 57.01 (s), 55.17 (s), 53.54 (s), 48.57 (s), 44.78 (s). MS(ESI): 457.2016 ($C_{29}H_{29}O_5$, $[M+H]^+$).

(E)-2-(2-(4-butoxystyryl)-4,6-dimethoxyphenyl)-6-methoxy-4H-chromen-4-one (***5r***). Yellow solid, Yield: 78%, Mp: 169-171 °C. IR (ATR Diamond Crystal, cm^{-1}): *v* 2959, 2900, 2869, 1637, 1592, 1568, 1334, 1198, 1153, 1076, 1016, 849, 826; ^{1}H NMR (600 MHz, DMSO) δ 7.57 (dd, *J* = 9.1, 1.2 Hz, 1H), 7.45 (d, *J* = 2.9 Hz, 1H), 7.36 (ddd, *J* = 9.1, 3.0, 1.3 Hz, 1H), 7.32 (d, *J* = 7.8 Hz, 2H), 7.23 (d, *J* = 16.1 Hz, 1H), 7.00 (s, 1H), 6.85-6.80 (m, 3H), 6.62 (s, 1H), 6.26 (s, 1H), 3.91-3.89 (m, 2H), 3.88 (d, *J* = 0.7 Hz, 3H), 3.86 (d, *J* = 1.0 Hz, 3H), 3.75 (s, 3H), 1.65-1.59 (m, 2H), 1.36 (tt, *J* = 13.7, 3.7 Hz, 2H), 0.87 (td, *J* = 7.4, 1.3 Hz,3H). ^{13}C NMR (101 MHz, $CDCl_3$): δ 186.21 (s), 171.65 (s), 162.87 (s), 160.24 (s), 157.29 (s), 143.98 (s), 141.75 (s), 139.82 (s), 135.28 (s), 134.13 (s), 129.36(s), 128.94 (s), 127.18 (s), 124.41 (s), 123.45 (s), 122.63 (s), 119.54 (s), 114.86 (s), 110.05 (s), 101.75 (s), 99.90 (s), 65.49 (s), 56.51 (s), 52.57 (s), 50.12 (s),48.02 (s), 44.57 (s),14.78 (s). MS(ESI): 487.2115 ($C_{30}H_{31}O_6$, $[M+H]^+$).

(E)-6-bromo-2-(2-(4-butoxystyryl)-4,6-dimethoxyphenyl)-4H-chromen-4-one (***5s***). Yellow solid, Yield: 79%, Mp: 265-267 °C. IR (ATR Diamond Crystal, cm^{-1}): *v* 2959, 2900, 1652, 1597, 1567, 1459, 1331, 1248, 1160, 1082, 963, 797; ^{1}H NMR (600 MHz, DMSO) δ 8.14 (d, *J* = 2.3 Hz, 1H), 7.93-7.90 (m, 1H), 7.60 (d, *J* = 8.9 Hz, 1H), 7.36 (d, *J* = 8.5 Hz, 2H), 7.24 (d, *J* = 16.1 Hz, 1H), 6.99 (d, *J* = 16.5 Hz, 1H), 6.87 (t, *J* = 12.4 Hz, 1H), 6.83 (d, *J* = 8.5 Hz, 2H), 6.62 (s, 1H), 6.34 (s, 1H), 3.90 (dd, *J* = 10.9, 4.3 Hz, 2H), 3.88 (s, 3H), 3.75 (s, 3H), 1.66-1.60 (m, 2H), 1.41-1.34 (m, 2H), 0.88 (t, *J* = 7.4 Hz, 3H). ^{13}C NMR (101 MHz,

$CDCl_3$): δ 181.91 (s), 162.65 (s), 157.27 (s), 156.08 (s), 155.09 (s), 140.48 (s), 139.05 (s), 138.67 (s), 137.28 (s), 130.53 (s), 128.63 (s), 128.94 (s), 127.08 (s), 121.91 (s), 120.86 (s), 120.13 (s), 118.74 (s), 115.16 (s), 110.65 (s), 105.35 (s), 98.90 (s), 66.19 (s), 57.11 (s), 55.27 (s), 53.62 (s), 52.12 (s), 15.28 (s). MS(ESI): 557.0834 ($C_{29}H_{27}BrO_5Na$, $[M+Na]^+$).

(E)-2-(2-(4-(benzyloxy)styryl)-4,6-dimethoxyphenyl)-4H-chromen-4-one (***5t***). Yellow solid, Yield: 92%, Mp: 156-157 °C. IR (ATR Diamond Crystal, cm^{-1}): *v* 2970, 2900, 1656, 1595, 1572, 1462, 1315, 1215, 1172, 1079, 830, 776; ^{1}H NMR (600 MHz, DMSO) δ 8.08 (d, *J* = 7.9 Hz, 1H), 7.80-7.74 (m, 1H), 7.59 (t, *J* = 9.9 Hz, 1H), 7.50 (t, *J* = 7.5 Hz, 1H), 7.36 (dt, *J* = 14.2, 7.5 Hz, 6H), 7.29 (t, *J* = 7.2 Hz, 1H), 7.24 (d, *J* = 16.1 Hz, 1H), 7.01 (s, 1H), 6.92 (d, *J* = 8.6 Hz, 2H), 6.88 (d, *J* = 16.1 Hz, 1H), 6.63 (s, 1H), 6.28 (s, 1H), 5.73 (s, 1H), 5.08-5.01 (m, 2H), 3.89 (s, 3H), 3.75 (s, 3H). ^{13}C NMR (101 MHz, $CDCl_3$): δ 181.91 (s), 162.65 (s), 160.27 (s), 159.48 (s), 157.09 (s), 156.48 (s), 152.05 (s), 151.67 (s), 145.28 (s),140.05 (s), 139.67 (s), 136.28 (s), 131.53 (s), 129.33 (s), 128.04 (s), 127.98 (s), 122.91 (s), 122.86 (s), 120.63 (s), 117.74 (s), 114.66 (s), 110.75 (s), 101.35 (s), 97.90 (s), 63.49 (s), 56.01 (s), 55.57 (s). MS(ESI): 491.1853 ($C_{32}H_{27}O_5$, $[M+H]^+$).

(E)-2-(2-(4-(benzyloxy)styryl)-4,6-dimethoxyphenyl)-6-methoxy-4H-chromen-4-one (***5u***). Yellow solid, Yield: 76%, Mp: 231-232 °C. IR (ATR Diamond Crystal, cm^{-1}): *v* 2969, 2900, 1635, 1570, 1486, 1452, 1337, 1076, 1030, 968, 847, 697; ^{1}H NMR (600 MHz, DMSO) δ 7.57 (d, *J* = 9.1 Hz, 1H), 7.45 (d, *J* = 3.1 Hz, 1H), 7.38 (dd, *J* = 10.1, 5.2 Hz, 3H), 7.36-7.31 (m, 4H), 7.29 (t, *J* = 7.0 Hz, 1H), 7.24 (d, *J* = 16.1 Hz, 1H), 7.00 (d, *J* = 2.0 Hz, 1H), 6.92 (d, *J* = 8.8 Hz, 2H), 6.86-6.81 (m, 1H), 6.62 (d, *J* = 2.1 Hz, 1H), 6.26 (s, 1H), 5.04 (d, *J* = 8.0 Hz, 2H), 3.88 (s, 3H), 3.86 (s, 3H), 3.75 (s, 3H). ^{13}C NMR (101 MHz, $CDCl_3$): δ 181.67 (s), 163.72 (s), 160.62 (s), 158.98 (s), 157.19 (s), 156.36 (s), 152.17 (s), 150.81 (s), 145.28 (s), 140.05 (s), 138.82 (s), 136.28 (s), 131.53 (s), 129.33 (s), 128.04 (s), 127.98 (s), 122.91 (s), 122.86 (s), 120.63 (s), 117.74 (s), 114.66 (s), 110.75 (s), 101.35 (s), 97.90 (s), 66.52 (s), 56.91 (s), 53.61 (s), 45.91. MS(ESI): 521.1959 ($C_{33}H_{29}O_6$, $[M+H]^+$).

(E)-2-(2-(4-(benzyloxy)styryl)-4,6-dimethoxyphenyl)-6-bromo-4H-chromen-4-one (***5v***).

Yellow solid, Yield: 78%, Mp: 259-260 °C. IR (ATR Diamond Crystal, cm^{-1}): *v* 2988, 2900, 1654, 1597, 1453, 1393, 1239, 1084, 974, 810; ^{1}H NMR (600 MHz, DMSO) δ 8.14 (d, *J* = 2.5 Hz, 1H), 7.93 (dd, *J* = 8.9, 2.5 Hz, 1H), 7.59 (t, *J* = 11.9 Hz, 1H), 7.41-7.37 (m, 4H), 7.35 (t, *J* = 7.5 Hz, 2H), 7.29 (t, *J* = 7.3 Hz, 1H), 7.24 (d, *J* = 16.1 Hz, 1H), 7.00 (t, *J* = 6.8 Hz, 1H), 6.92 (d, *J* = 8.8 Hz, 2H), 6.89 (d, *J* = 16.2 Hz, 1H), 6.62 (d, *J* = 2.0 Hz, 1H), 6.33 (s, 1H), 5.73 (s, 1H), 5.06 (s, 2H), 3.88 (s, 3H), 3.75 (s, 3H). ^{13}C NMR (101 MHz, $CDCl_3$): δ 182.69 (s), 164.92 (s), 161.82 (s), 157.54 (s), 157.01 (s), 156.36 (s), 152.17 (s), 150.81 (s), 145.28 (s),140.05 (s), 138.92 (s), 136.28 (s), 131.53 (s), 129.33 (s), 128.14 (s), 127.26 (s), 122.73 (s), 122.86 (s), 121.63 (s), 117.52 (s), 114.74 (s), 110.16 (s), 101.54 (s), 100.83 (s), 67.62 (s), 55.73 (s), 50.96 (s). MS(ESI): 591.0778 ($C_{32}H_{25}BrO_5Na$, $[M+Na]^+$).

*4.4 Synthesis of resveratrol-based flavonol derivatives (**7a**~**7o**)*

In a 50 mL round-bottom flask, a solution of compounds **6a**~**6o** (1 mmol, 1.0 equiv) in methanol was added NaOH (5 mmol, 5.0 equiv) and 30% H_2O_2 (5 mmol, 5.0 equiv), the mixture was stirred at 40 °C until the reaction was completed. The reaction was cooled back to room temperature and added ice-water, it was added hydrochloric acid to adjust pH to neutral. The suspension was then stirred and vacuum filtered to provide the residue, the crude product was purified by column chromatography on silica gel to obtained the desired compounds.

(E)-2-(2,4-dimethoxy-6-(4-methoxystyryl)phenyl)-3-hydroxy-4H-chromen-4-one (***7a***). White solid, Yield: 76%, Mp: 230-232 °C. 1H NMR (600 MHz, DMSO): *δ* 8.85 (s, 1H), 8.15 (d, *J*= 8.0 Hz, 1H), 7.74 (t, *J* = 7.7 Hz, 1H), 7.60 (d, *J* = 8.4 Hz, 1H), 7.46 (t, *J* = 7.5 Hz, 1H), 7.30 (d, *J* = 8.6 Hz, 2H), 7.25 (d, *J* = 16.2 Hz, 1H), 7.03 (s, 1H), 6.84 (d, *J* = 8.6 Hz, 2H), 6.74 (d, *J* = 16.2 Hz, 1H), 6.61 (s, 1H), 3.89 (s, 3H), 3.72 (t, *J* = 20.0 Hz, 6H). ^{13}C NMR (151 MHz, DMSO): *δ* 175.66 (s), 164.97 (s), 162.31 (s), 161.96 (s), 158.47 (s), 148.85 (s), 143.43 (s), 141.68 (s), 136.50 (s), 133.97 (s), 132.35 (s), 131.01 (s), 128.08 (s), 127.54 (s), 125.75 (s), 125.28 (s), 121.55 (s), 117.30 (s), 114.78 (s), 104.04 (s), 100.93 (s), 59.01 (s), 58.66 (s), 58.19 (s). MS (ESI): 431.1483.($C_{26}H_{22}O_6$, $[M+H]^+$).

(E)-2-(2,4-dimethoxy-6-(4-methoxystyryl)phenyl)-3-hydroxy-7-methyl-4H-chromen-4-one (***7b***). White solid, Yield: 78%, Mp: 210-213 °C. ^{1}H NMR (600 MHz, DMSO): δ 8.77 (s, 1H), 8.02 (d, *J* = 8.2 Hz, 1H), 7.40 (s, 1H), 7.32 – 7.23 (m, 4H), 7.02 (s, 1H), 6.84 (d, *J* = 8.6 Hz, 2H), 6.71 (d, *J* = 16.2 Hz, 1H), 6.60 (s, 1H), 3.89 (s, 3H), 3.71 (t, *J* = 14.1 Hz, 6H), 2.42 (s, 3H). ^{13}C NMR (101 MHz, DMSO): δ 172.37 (s), 161.80 (s), 159.18 (s), 158.83 (s), 155.49 (s), 145.24 (s), 144.25 (s), 140.12 (s), 138.50 (s), 130.77 (s), 129.23 (s), 127.85 (s), 125.93 (s), 124.72 (s), 122.64 (s), 119.93 (s), 117.87 (s), 100.88 (s), 97.79 (s), 114.18 (s), 111.76 (s), 55.85 (s), 55.51 (s), 55.05 (s), 21.15 (s). MS(ESI): 445.1645.($C_{27}H_{24}O_6$, $[M+H]^+$).

(E)-2-(2,4-dimethoxy-6-(4-methoxystyryl)phenyl)-3-hydroxy-6-methyl-4H-chromen-4-one (***7c***). White solid, Yield: 44%, Mp: 201-204 °C. ^{1}H NMR (600 MHz, DMSO): δ 8.80 (s, 1H), 7.93 (s, 1H), 7.56 (d, *J* = 8.6 Hz, 1H), 7.49 (d, *J* = 8.5 Hz, 1H), 7.28 (d, *J* = 8.5 Hz, 2H), 7.25 (d, *J* = 16.2 Hz, 1H), 7.02 (s, 1H), 6.84 (d, *J* = 8.3 Hz, 2H), 6.69 (d, *J* = 16.2 Hz, 1H), 6.60 (s, 1H), 3.89 (s, 3H), 3.70 (d, *J* = 13.1 Hz, 6H), 2.44 (s, 3H). ^{13}C NMR (101 MHz, $CDCl_3$): δ 172.94(s), 162.46 (s), 159.59 (s), 159.29 (s), 154.69 (s), 144.74 (s), 139.83 (s), 139.54 (s), 134.80 (s), 134.32 (s), 131.18 (s), 129.63 (s), 128.04 (s), 124.57 (s), 123.31 (s), 121.01 (s), 118.44 (s), 114.09 (s), 111.35 (s), 101.26 (s), 98.00 (s), 56.03 (s), 55.73 (s), 55.43 (s), 20.98 (s). MS(ESI): 445.1642.($C_{27}H_{24}O_6$, $[M+H]^+$).

(E)-2-(2,4-dimethoxy-6-(4-methoxystyryl)phenyl)-3-hydroxy-6-methoxy-4H-chromen-4-one (***7d***). White solid, Yield: 89%, Mp: 188-191 °C. ^{1}H NMR (600 MHz, DMSO): δ 8.81 (s, 1H), 7.56 (d, *J* = 9.1 Hz, 1H), 7.48 (d, *J* = 2.7 Hz, 1H), 7.34 (dd, *J* = 9.1, 2.7 Hz, 1H), 7.29 (d, *J* = 8.4 Hz, 2H), 7.25 (d, *J* = 16.2 Hz, 1H), 7.02 (s, 1H), 6.84 (d, *J* = 8.4 Hz, 2H), 6.69 (d, *J* = 16.2 Hz, 1H), 6.60 (s, 1H), 3.88 (d, *J* = 8.5 Hz, 6H), 3.70 (d, *J* = 14.7 Hz, 6H). ^{13}C NMR (101 MHz, DMSO): δ 172.09 (s), 161.82 (s), 159.19 (s), 158.83 (s), 155.84 (s), 150.32 (s), 145.61 (s), 139.86 (s), 138.53 (s), 130.79 (s), 129.22 (s), 127.83 (s), 123.18 (s), 122.70 (s), 122.63 (s), 120.05 (s), 114.18 (s), 111.75 (s), 103.96 (s), 100.92 (s), 97.80 (s), 55.86 (s), 55.69 (s), 55.51 (s), 55.05 (s). MS(ESI): 461.1591.($C_{27}H_{24}O_7$, $[M+H]^+$).

(E)-2-(2,4-dimethoxy-6-(4-methoxystyryl)phenyl)-7-fluoro-3-hydroxy-4H-chromen-4-one (***7e***). White solid, Yield: 63%, Mp: 236-239 °C. ^{1}H NMR (600 MHz, DMSO): δ 8.94 (s, 1H), 8.20 (dd, *J* = 8.9, 6.5 Hz, 1H), 7.58 (dd, *J* = 9.7, 2.1 Hz, 1H), 7.37-7.34 (m, 1H), 7.33 (d, *J* = 8.6 Hz, 2H), 7.26 (d, *J* = 16.2 Hz, 1H), 7.03 (d, *J* = 1.6 Hz, 1H), 6.84 (d, *J* = 8.7 Hz, 2H), 6.74 (d, *J* = 16.2 Hz, 1H), 6.60 (d, *J* = 1.7 Hz, 1H), 3.89 (s, 3H), 3.71 (d, *J* = 13.5 Hz, 6H). ^{13}C NMR (101 MHz, $CDCl_3$): δ 172.46 (s), 167.96 (s), 164.28 (s), 162.62 (s), 159.67 (s), 159.29 (s), 157.37 (s), 145.24 (s), 139.81 (s), 139.62 (s), 131.43 (s), 129.57 (s), 128.17 (s), 123.16 (s), 118.43 (s), 114.13 (s), 110.84 (s), 105.15 (s), 104.90 (s), 101.34 (s), 97.95 (s), 56.01 (s), 55.56 (s), 55.30 (s). MS(ESI): 449.1392.($C_{26}H_{21}FO_6$, $[M+H]^+$).

(E)-2-(2,4-dimethoxy-6-(4-methoxystyryl)phenyl)-6-fluoro-3-hydroxy-4H-chromen-4-one (***7f***). White solid, Yield: 68%, Mp: 190-193 °C. ^{1}H NMR (600 MHz, DMSO): δ 8.99 (s, 1H), 7.80 (dd, *J* = 22.0, 16.1 Hz, 1H), 7.72 (dd, *J* = 8.9, 3.7 Hz, 1H), 7.64 (t, *J* = 7.1 Hz, 1H), 7.32 (d, *J* = 8.3 Hz, 2H), 7.26 (d, *J* = 16.2 Hz, 1H), 7.01 (d, *J* = 26.2 Hz, 1H), 6.82 (t, *J* = 16.7 Hz, 2H), 6.72 (d, *J* = 16.2 Hz, 1H), 6.61 (s, 1H), 3.89 (s, 3H), 3.70 (d, *J* = 15.6 Hz,6H). ^{13}C NMR (101 MHz, DMSO): δ 171.91 (s), 161.93 (s), 159.20 (s), 158.84 (s), 157.16 (s), 151.85 (s), 146.32 (s), 140.04 (s), 138.63 (s), 130.92 (s), 129.21 (s), 127.95 (s), 123.16 (s), 122.56 (s), 121.74 (s), 121.20 (s), 114.14 (s), 111.44 (s), 109.12 (s), 100.95 (s), 97.78 (s), 55.88 (s), 55.52 (s), 55.05 (s). MS(ESI): 449.1392.($C_{26}H_{21}FO_6$, $[M+H]^+$).

(E)-8-chloro-2-(2,4-dimethoxy-6-(4-methoxystyryl)phenyl)-3-hydroxy-4H-chromen-4-one (***7g***). White solid, Yield: 55%, Mp: 208-210 °C. ^{1}H NMR (600 MHz, DMSO): δ 9.07 (s, 1H), 8.11 (d, *J* = 8.0 Hz, 1H), 7.92 (d, *J* = 7.7 Hz, 1H), 7.45 (t, *J* = 7.9 Hz, 1H), 7.34 (d, *J* = 8.5 Hz, 2H), 7.27 (d, *J* = 16.2 Hz, 1H), 7.04 (s, 1H), 6.84 (d, *J* = 8.5 Hz, 2H), 6.79 (d, *J* = 16.2 Hz, 1H), 6.63 (s, 1H), 3.90 (s, 3H), 3.74 (s, 3H), 3.70 (s, 3H). ^{13}C NMR (151 MHz, DMSO): δ 175.28 (s), 165.16 (s), 162.33 (s), 162.18 (s), 153.80 (s), 149.10 (s), 143.72 (s), 141.98 (s), 136.44 (s), 134.08 (s), 132.43 (s), 131.14 (s), 127.87 (s), 127.27 (s), 126.80 (s), 125.84 (s), 125.06 (s), 117.26 (s), 114.39 (s), 104.34 (s), 101.12 (s), 59.17 (s), 58.69 (s), 58.21 (s). MS(ESI): 465.1097.($C_{26}H_{21}ClO_6$, $[M+H]^+$).

(E)-7-chloro-2-(2,4-dimethoxy-6-(4-methoxystyryl)phenyl)-3-hydroxy-4H-chromen-4-one (***7h***). White solid, Yield: 48%, Mp: 209-210 °C. ^{1}H NMR (600 MHz, DMSO): δ 8.98 (s, 1H), 8.14 (d, *J* = 8.7 Hz, 1H), 7.82 (d, *J* = 1.5 Hz, 1H), 7.50 (dd, *J* = 8.6, 1.7 Hz, 1H), 7.33 (d, *J* = 8.7 Hz, 2H), 7.25 (d, *J* = 16.2 Hz, 1H), 7.03 (d, *J* = 1.7 Hz, 1H), 6.84 (d, *J* = 8.7 Hz, 2H), 6.73 (t, *J* = 12.4 Hz, 1H), 6.60 (d, *J* = 1.8 Hz, 1H), 3.89 (s, 3H), 3.71 (d, *J* = 13.0 Hz, 6H). ^{13}C NMR (101 MHz, $CDCl_3$): δ 172.52 (s), 162.63 (s), 159.67 (s), 159.30 (s), 156.40 (s), 145.31 (s), 140.07 (s), 139.63 (s), 139.52 (s), 131.48 (s), 129.54 (s), 128.08 (s), 126.88 (s), 125.40 (s), 123.10 (s), 120.08 (s), 118.62 (s), 114.13 (s), 110.80 (s), 101.33 (s), 97.93 (s), 56.00 (s), 55.56 (s), 55.30 (s). MS(ESI): 465.1102.($C_{26}H_{21}ClO_6$, $[M+H]^+$).

(E)-6-chloro-2-(2,4-dimethoxy-6-(4-methoxystyryl)phenyl)-3-hydroxy-4H-chromen-4-one (***7i***). White solid, Yield: 60%, Mp: 189-192°C. ^{1}H NMR (600 MHz, $CDCl_3$): δ 8.27 (s, 1H), 7.60 (d, *J* = 9.0 Hz, 1H), 7.45 (d, *J* = 8.9 Hz, 1H), 7.26 (d, *J* = 4.7 Hz, 3H), 7.06 (d, *J* = 16.0 Hz, 1H), 6.91 (s, 1H), 6.80 (d, *J* = 8.2 Hz, 2H), 6.77 (d, *J* = 16.1 Hz, 1H), 6.50 (s, 1H), 3.93 (s, 3H), 3.78 (d, *J* = 6.5 Hz, 6H). ^{13}C NMR (101 MHz, $CDCl_3$): δ 172.35 (s), 162.65 (s), 159.68 (s), 159.27 (s), 154.65 (s), 145.45 (s), 140.02 (s), 139.63 (s), 133.60 (s), 131.45 (s), 130.34 (s), 129.51 (s), 128.04 (s), 124.74 (s), 123.08 (s), 122.35 (s), 120.41 (s), 114.13 (s), 110.78 (s), 101.36 (s), 97.93 (s), 56.01 (s), 55.57 (s), 55.31(s). MS(ESI): 465.1101. ($C_{26}H_{21}ClO_6$, $[M+H]^+$).

(E)-7-bromo-2-(2,4-dimethoxy-6-(4-methoxystyryl)phenyl)-3-hydroxy-4H-chromen-4-one (***7j***). White solid, Yield: 76%, Mp: 202-205°C. ^{1}H NMR (600 MHz, DMSO): δ 9.03 (s, 1H), 8.05 (d, *J* = 8.6 Hz, 1H), 7.94 (d, *J* = 1.3 Hz, 1H), 7.63 (dd, *J* = 8.6, 1.1 Hz, 1H), 7.33 (d, *J* = 8.6 Hz, 2H), 7.25 (d, *J* = 16.2 Hz, 1H), 7.01 (d, *J* = 1.5 Hz, 1H), 6.83 (d, *J* = 8.6 Hz, 2H), 6.73 (d, *J* = 16.2 Hz, 1H), 6.59 (d, *J* = 1.6 Hz, 1H), 3.88 (s, 3H), 3.70 (d, *J* = 11.5 Hz, 6H). ^{13}C NMR (101 MHz, $CDCl_3$): δ 172.60 (s), 162.64 (s), 159.68 (s), 159.30 (s), 156.34 (s), 145.17 (s), 140.09 (s), 139.63 (s), 131.49 (s), 129.54 (s), 128.08 (s), 127.76 (s), 126.89 (s), 123.09 (s), 121.71 (s), 120.41 (s), 114.13 (s), 110.78 (s), 101.32 (s), 97.93 (s), 56.01 (s), 55.56 (s), 55.31 (s). MS(ESI): 509.0590.($C_{26}H_{21}BrO_6$, $[M+H]^+$).

(E)-6-bromo-2-(2,4-dimethoxy-6-(4-methoxystyryl)phenyl)-3-hydroxy-4H-chromen-4-one (***7k***). White solid, Yield: 82%, Mp: 201-204 °C. ^{1}H NMR (600 MHz, DMSO): δ 9.08 (s, 1H), 8.22 (d, *J* = 2.4 Hz, 1H), 7.88 (dd, *J* = 8.9, 2.4 Hz, 1H), 7.61 (d, *J* = 8.9 Hz, 1H), 7.33 (d, *J* = 8.7 Hz, 2H), 7.26 (d, *J* = 16.2 Hz, 1H), 7.03 (d, *J* = 1.7 Hz, 1H), 6.84 (d, *J* = 8.7 Hz, 2H), 6.72 (d, *J* = 16.2 Hz, 1H), 6.60 (d, *J* = 1.8 Hz, 1H), 3.89 (s, 3H), 3.70 (d, *J* = 11.1 Hz, 6H). ^{13}C NMR (101 MHz, $CDCl_3$): δ 171.92 (s), 162.65 (s), 159.68 (s), 159.28 (s), 155.08 (s), 145.54 (s), 140.10 (s), 139.63 (s), 136.28 (s), 131.45 (s), 129.51 (s), 128.04 (s), 123.07 (s), 122.89 (s), 120.62 (s), 117.74 (s), 114.13 (s), 110.79 (s), 101.36 (s), 97.93 (s), 56.01 (s), 55.57 (s), 55.31 (s). MS(ESI): 511.0572.($C_{26}H_{21}BrO_6$, $[M+H]^+$).

(E)-2-(2,4-dimethoxy-6-(4-methoxystyryl)phenyl)-3-hydroxy-6,7-dimethyl-4H-chromen-4-one (***7l***). White solid, Yield: 66%, Mp: 214-217 °C. ^{1}H NMR (600 MHz, $CDCl_3$): δ 8.03 (s, 1H), 7.27 (d, *J* = 6.3 Hz, 1H), 7.26 (s, 1H), 7.25 (s, 2H), 7.06 (d, *J* = 16.0 Hz, 1H), 6.91 (s, 1H), 6.82-6.77 (m, 3H), 6.50 (d, *J* = 1.4 Hz, 1H), 3.92 (d, *J* = 8.1 Hz, 3H), 3.77 (d, *J* = 3.9 Hz, 6H), 2.39 (d, *J* = 7.5 Hz, 6H). ^{13}C NMR (101 MHz, $CDCl_3$): δ 172.88 (s), 162.39 (s), 159.57 (s), 159.31 (s), 155.16 (s), 144.27 (s), 144.00 (s), 139.68 (s), 139.50 (s), 133.84 (s), 131.09 (s), 129.67 (s), 128.05 (s), 124.83 (s), 123.36 (s), 119.38 (s), 118.67 (s), 114.08 (s), 111.52 (s), 101.20 (s), 98.00 (s), 56.02 (s), 55.54 (s), 55.29 (s), 20.55 (s), 19.39 (s). MS(ESI): 459.1803.($C_{28}H_{26}O_6$, $[M+H]^+$).

(E)-2-(2-(4-ethoxystyryl)-4,6-dimethoxyphenyl)-3-hydroxy-4H-chromen-4-one (***7m***). White solid, Yield: 77%, Mp: 244-247 °C. ^{1}H NMR (600 MHz, $CDCl_3$): δ 8.31 (d, *J* = 7.9 Hz, 1H), 7.66 (dd, *J* = 11.4, 4.2 Hz, 1H), 7.50 (d, *J* = 8.5 Hz, 1H), 7.43 (t, *J* = 7.5 Hz, 1H), 7.26 (s, 1H), 7.24 (s, 1H), 7.07 (d, *J* = 16.1 Hz, 1H), 6.92 (d, *J* = 2.0 Hz, 1H), 6.81 (d, *J* = 16.2 Hz, 1H), 6.78 (d, *J* = 8.7 Hz, 2H), 6.51 (d, *J* = 2.0 Hz, 1H), 6.29 (s, 1H), 3.99 (q, *J* = 7.0 Hz, 2H), 3.93 (s, 3H), 3.79 (s, 3H), 1.38 (t, *J* = 7.0 Hz, 3H). ^{13}C NMR (101 MHz, $CDCl_3$): δ 173.15 (s), 162.51 (s), 159.31 (s), 159.01 (s), 156.42 (s), 145.02 (s), 139.93 (s), 139.63 (s), 133.32 (s), 131.35 (s), 129.45 (s), 128.06 (s), 125.54 (s), 124.38 (s), 123.14 (s), 121.55 (s), 118.69 (s), 114.64 (s), 111.22 (s), 101.30 (s), 97.96 (s), 63.47 (s), 56.02 (s), 55.55 (s), 14.79 (s). MS(ESI): 445.1642.($C_{27}H_{24}O_6$, $[M+H]^+$).

(E)-2-(2-(4-ethoxystyryl)-4,6-dimethoxyphenyl)-3-hydroxy-6-methoxy-4H-chromen-4-one (***7n***). White solid, Yield: 81%, Mp: 220-223 °C. ^{1}H NMR (600 MHz, $CDCl_3$): δ 7.63 (d, J = 3.0 Hz, 1H), 7.44-7.42 (m, 1H), 7.27 (dd, J = 9.2, 3.1 Hz, 1H), 7.24 (d, J = 8.7 Hz, 2H), 7.05 (d, J = 16.1 Hz, 1H), 6.91 (d, J = 2.1 Hz, 1H), 6.78 (dd, J = 12.4, 3.6 Hz, 3H), 6.50 (d, J = 2.1 Hz, 1H), 6.28 (s, 1H), 3.99 (q, J = 7.0 Hz, 2H), 3.93 (d, J = 6.1 Hz, 6H), 3.78 (s, 3H), 1.38 (t, J = 7.0 Hz, 3H). ^{13}C NMR (101 MHz, $CDCl_3$): δ 172.71 (s), 162.47 (s), 159.29 (s), 159.00 (s), 156.41 (s), 151.58 (s), 144.80 (s), 139.62 (s), 139.54 (s),131.28 (s), 129.44 , 128.03 (s), 124.15 (s), 123.14 (s), 121.94 (s), 120.16 (s), 114.63 (s), 111.27 (s), 103.82 (s), 101.26 (s), 97.95 (s), 63.46 (s), 56.02 (s), 56.00 (s), 55.55 (s), 14.79 (s). MS(ESI): 475.1747. ($C_{28}H_{26}O_7$, $[M+H]^+$).

(E)-6-bromo-2-(2-(4-ethoxystyryl)-4,6-dimethoxyphenyl)-3-hydroxy-4H-chromen-4-one (***7o***). White solid, Yield: 78%, Mp: 200-205 °C. ^{1}H NMR (600 MHz, $CDCl_3$): δ 8.44 (d, J = 2.4 Hz, 1H), 7.73 (dd, J = 9.0, 2.4 Hz, 1H), 7.39 (d, J = 8.9 Hz, 1H), 7.24 (d, J = 9.0 Hz, 2H), 7.06 (d, J = 16.0 Hz, 1H), 6.90 (d, J = 2.1 Hz, 1H), 6.79 (d, J = 8.7 Hz, 2H), 6.76 (d, J = 16.1 Hz, 1H), 6.50 (d, J = 2.1 Hz, 1H), 6.22 (s, 1H), 4.00 (q, J = 7.0 Hz, 2H), 3.93 (s, 3H), 3.78 (s, 3H), 1.38 (t, J = 7.0 Hz, 3H). ^{13}C NMR (101 MHz, $CDCl_3$): δ 171.91 (s), 162.65 (s), 159.27 (s), 159.08 (s), 155.09 (s), 145.48 (s), 140.05 (s), 139.67 (s), 136.28 (s), 131.53 (s), 129.33 (s), 128.04 (s), 127.98 (s), 122.91 (s), 122.86 (s), 120.63 (s), 117.74 (s), 114.66 (s), 110.75 (s), 101.35 (s), 97.90 (s), 63.49 (s), 56.01 (s), 55.57 (s), 14.78 (s). MS(ESI): 525.0729.($C_{27}H_{23}BrO_6$, $[M+H]^+$).

4.5 Cell culture

Mouse peritoneal macrophages were obtained from BeNa Culture Collection Company. RAW264.7 cells were cultured in DMEM (Hyclone, USA) supplemented with 10% FBS (Biological Industries, Israel, 100 U/mL penicillin and100 μg/mL streptomycin (Beyotime) at 37 °C in a humidified atmosphere containing 5% CO_2.

4.6 Determination secretion of NO, TNF-α and IL-6

RAW264.7 cells were seeded into 48-well plate with 6×10^4 cells per well and

incubated for 24 h. RAW264.7 cells were pretreated with compounds (10 μM) for 1 h, incubated with LPS (0.5 μg/mL) for 24 h. The supernatants were collected and examined for NO production using Griess reagent (Beyotime, China). The levels of TNF-α and IL-6 in the culture medium were measured by ELISA (eBioScience, San Diego, CA).

4.7 Cell viability assay (MTT)

RAW264.7 cells were seeded into 96-well plate with 6×10^4 cells per well and maintained at 37 °C in 5% CO_2 about 24 h. RAW264.7 cells were pretreated with all compounds (20 μM) for 1 h, incubated with LPS (0.5 μg/mL) for 24 h. After incubation at 37 °C for 4 h, the culture media containing MTT (prepared in PBS solution, 5 mg/mL) were removed, and then DMSO (150 μL) was added into per well and the absorbance at 492 nm was measured by a microplate reader (MQX200, Bio-Tek, USA).

4.8 Western blotting

RAW264.7 cells were seeded into 96-well plate with 3×10^5 cells per well and maintained at 37°C in 5% CO_2 about 24 h. RAW264.7 cells were pretreated with compound **7f** (2, 1, 0.5 μM) for 1 h, incubated with LPS (0.5 μg/mL) for 0.5 h. The cells were lysed in 300 μL RIPA cell lysis buffer (Contains PMSF and phosphatase inhibitors, Beyotime china) and incubated on ice for 30 min. proteins were run on 12% SDS-PAGE and then transferred to PVDF membrane (GE Healthcare, UK). The blotted membrane incubated with specific primary antibodies (all antibody obtain from cell signaling Technology, USA) overnight at 4°C. The membranes were washed in TBST (Beyotime Biotech, Nantong, China), incubated with a 1:5000 dilutions of HRP-conjugated secondary antibody (Beyotime Biotech, Nantong, China) for 1h at room temperature.

4.9 *In vivo experiment*

The 40 male C57BL/6 mice weighing 18~22 g were purchased from Animal Department of Anhui Medical University. After one-week acclimatization, mice were randomly divided into four groups on average, including the control group, LPS group, compound **7f** (10 mg/kg) +LPS group and compound **7f** (20 mg/kg) +LPS group.

30 min before a 20 mg/kg LPS tail vein injection. Control group animals were received only an equal volume of saline by Intraperitoneal injection. Mice were anesthetized and sacrificed 48 h after LPS injection. Lung tissues were harvested for experiment. Lung tissue were fixed in 4% paraformaldehyde solution, embedded in paraffin. After dehydration, sections were stained with hematoxylin and eosin (H&E) and immunohistochemistry according to the previously reported method. The upper lung lobe of the right lungs was excised, and obtain a wet weight. The lungs were then placed in an oven at 60 °C for exceed 48 h until the dry weight was constant. Lung wet/dry weight ratio was calculated to assess tissue edema. The lung tissue MPO activity was assessed using a kit (Jiancheng Bioengineering Institute, Nanjing, China) following the manufacturer's instruction. The research was approved by the Ethics Committee of Anhui Medical University on the care.

4.10 Statistical analysis

Data are expressed as means±SEM and were analyzed statistically by analysis of variance (ANOVE). A value of $p<0.05$ was considered to be statistically significant. All experiments date were repeated at least three times.

Acknowledgments

The authors wish to thank the National Natural Science Foundation of China (No. 21572003, 21272008).

Supporting information

Spectral data of representative compounds containing ^{1}H NMR, ^{13}C NMR and HRMS. CCDC-1551040 (compound **5r**) and CCDC-1551039 (compound **5u**) contain the supplementary crystallographic data for this paper. These data can be obtained free of charge via the URL http:// www.ccdc.cam.ac.uk/conts/retrieving. (or from the CCDC, 12 Union Road, Cambridge CB2 1EZ, UK; fax: (+44) 1223 336033; e-mail: deposit@ccdc.cam.ac.uk). Tables S1~S11 and Figures S1~S15 are available free of charge.

References and notes

[1] Z. Liu, L. Tang, H. Zhu, T. Xu, C. Qiu, S. Zheng, Y. Gu, J. Feng, Y. Zhang, G. Liang, Design, Synthesis, and Structure-Activity Relationship Study of Novel Indole-2-carboxamide Derivatives as Anti-inflammatory Agents for the Treatment of Sepsis, J. Med. Chem., 59 (2016) 4637-4650.

[2] G. Chen, Y. Zhang, X. Liu, Q. Fang, Z. Wang, L. Fu, Z. Liu, Y. Wang, Y. Zhao, X. Li, G. Liang, Discovery of a New Inhibitor of Myeloid Differentiation 2 from Cinnamamide Derivatives with Anti-Inflammatory Activity in Sepsis and Acute Lung Injury, J. Med. Chem., 59 (2016) 2436-2451.

[3] W. Albrecht, A. Unger, S.M. Bauer, S.A. Laufer, Discovery of N-{4-[5-(4-Fluorophenyl)-3-methyl-2-methylsulfanyl-3H-imidazol-4-yl]-pyridin-2-yl }-ac etamide (CBS-3595), a Dual p38alpha MAPK/PDE-4 Inhibitor with Activity against TNFalpha-Related Diseases, J. Med. Chem., 60 (2017) 5290-5305

[4] F. Imam, N.O. Al-Harbi, M.M. Al-Harbi, M.A. Ansari, K.M. Zoheir, M. Iqbal, M.K. Anwer, A.R. Al Hoshani, S.M. Attia, S.F. Ahmad, Diosmin downregulates the expression of T cell receptors, pro-inflammatory cytokines and NF-kappaB activation against LPS-induced acute lung injury in mice, Pharmacol Res, 102 (2015) 1-11.

[5] J. Cohen, The immunopathogenesis of sepsis, Nature, 420 (2002) 885-891.

[6] W. Schulte, J. Bernhagen, R. Bucala, Cytokines in sepsis: potent immunoregulators and potential therapeutic targets--an updated view, Mediators Inflamm, 2013 (2013) 165974.

[7] L. Chen, Y. Jin, W. Fu, S. Xiao, C. Feng, B. Fang, Y. Gu, C. Li, Y. Zhao, Z. Liu, G. Liang, Design, Synthesis, and Structure-Activity Relationship Analysis of Thiazolo[3,2-a]pyrimidine Derivatives with Anti-inflammatory Activity in Acute Lung Injury, ChemMedChem, 12 (2017) 1022-1032.

[8] O. Brattstrom, F. Granath, P. Rossi, A. Oldner, Early predictors of morbidity and mortality in trauma patients treated in the intensive care unit, Acta Anaesthesiol Scand, 54 (2010) 1007-1017.

[9] G.D. Rubenfeld, E. Caldwell, E. Peabody, J. Weaver, D.P. Martin, M. Neff, E.J. Stern, L.D. Hudson, Incidence and outcomes of acute lung injury, N Engl J Med, 353 (2005) 1685-1693.

[10] M. Naffaa, B.F. Makhoul, A. Tobia, M. Kaplan, D. Aronson, W. Saliba, Z.S. Azzam, Interleukin-6 at discharge predicts all-cause mortality in patients with sepsis, Am J Emerg Med, 31 (2013) 1361-1364.

[11] S. Lv, M. Han, R. Yi, S. Kwon, C. Dai, R. Wang, Anti-TNF-alpha therapy for patients with sepsis: a systematic meta-analysis, Int J Clin Pract, 68 (2014) 520-528.

[12] E.R. Johnson, M.A. Matthay, Acute lung injury: epidemiology, pathogenesis, and treatment, J Aerosol Med Pulm Drug Deliv, 23 (2010) 243-252.

[13] Y. Koh, Update in acute respiratory distress syndrome, J Intensive Care, 2 (2014) 2.

[14] J. Pan, T. Xu, F. Xu, Y. Zhang, Z. Liu, W. Chen, W. Fu, Y. Dai, Y. Zhao, J. Feng, G. Liang, Development of resveratrol-curcumin hybrids as potential therapeutic agents for inflammatory lung diseases, Eur J Med Chem, 125 (2017) 478-491.

[15] L. Chen, H. Chen, P. Chen, W. Zhang, C. Wu, C. Sun, W. Luo, L. Zheng, Z. Liu, G. Liang, Development of 2-amino-4-phenylthiazole analogues to disrupt myeloid differentiation factor 88 and prevent inflammatory responses in acute lung injury, Eur J Med Chem, 161 (2019) 22-38.

[16] F. Di Padova, V.F.J. Quesniaux, B. Ryffel, MyD88 as a therapeutic target for inflammatory lung diseases, Expert Opin Ther Targets, 22 (2018) 401-408.

[17] T. Ve, P.R. Vajjhala, A. Hedger, T. Croll, F. DiMaio, S. Horsefield, X. Yu, P. Lavrencic, Z. Hassan, G.P. Morgan, A. Mansell, M. Mobli, A. O'Carroll, B. Chauvin, Y. Gambin, E. Sierecki, M.J. Landsberg, K.J. Stacey, E.H. Egelman, B. Kobe, Structural basis of TIR-domain-assembly formation in MAL- and MyD88-dependent TLR4 signaling, Nat Struct Mol Biol, 24 (2017) 743-751.

[18] J. A. Baur, D. A. Sinclair, Therapeutic potential of resveratrol: the *in vivo* evidence. Nat Rev Drug Discov, 5 (2006) 493-506.

[19] F. Lolicato, A. Raudino, D. Milardi, R. C. La, Resveratrol interferes with the aggregation of membrane-bound human-IAPP: A molecular dynamics study, Eur J Med Chem, 92 (2015) 876-81.

[20] G. X. Wang, Z. Q. Hu, Q. T. Fu, S. Xu, Q. K. Cui, R. Y. Jia, Y. F. Zou, C. L. He, L. X. Li, Z. Q. Yin, Resveratrol mitigates lipopolysaccharide-mediated acute inflammation in rats by inhibiting the TLR4/ NF-κB p65/MAPKs signaling cascade, Sci Rep, 7 (2017)

45006.

[21] M. L.Tang, C. Zhong, Z. Y. Liu, P. Peng, X. H. Liu, X. Sun, Discovery of novel sesquistilbene indanone analogues as potent anti-inflammatory agents, Eur J Med Chem, 113 (2016) 63-74.

[22] B. F. Ruan, W. W. Ge, H. J. Cheng, Q. S. Li, X. H. Liu, Resveratrol-based cinnamic ester hybrids: synthesis, characterization and anti-inflammatory activity, J Enzym Inhib Med Ch, 32 (2017) 1282-1290.

[23] D. C. Zimmermann-Franco, B. Esteves, L. M. Lacerda, I. O. Souza, J. A. Dos Santos, N. C. C. Pinto, E. Scio, A. D. Da Silva, G. C. Macedo, In vitro and in vivo anti-inflammatory properties of imine resveratrol analogues, Bioorg Med Chem, 26 (2018) 4898-4906.

[24] D. C. Zimmermann-Franco, B. Esteves, L. M. Lacerda, I. O. Souza, J. A. Dos Santos, N. C. C. Pinto, E. Scio, A. D. Da Silva, G. C. Macedo, In *vitro* and in *vivo* anti-inflammatory properties of imine resveratrol analogues, Bioorg Med Chem, 26 (2018) 4898-4906.

[25] Z. Safaeinejad, F. Kazeminasab, A. Kiani-Esfahani, K. Ghaedi, M. Hossein Nasr-Esfahani, Multi-effects of Resveratrol on stem cell characteristics: Effective dose, time, cell culture conditions and cell type-specific responses of stem cells to Resveratrol, Eur J Med Chem, 155 (2018) 651-657.

[26] D. Şöhretoğlua, S. Sarib, B. Barutc, A. Özelc, Tyrosinase inhibition by some flavonoids: Inhibitory activity, mechanism by in *vitro* and in silico studies, Bioorg Chem , 81 (2018) 168-174.

[27] K. Pawlowska, M. E. Czerwinska, M. Wilczek, J. Strawa, M. Tomczyk, S. Granica, Anti-inflammatory Potential of Flavonoids from the Aerial Parts of Corispermum marschallii, J Nat Prod, 81 (2018) 1760-1768.

[28] C. Spagnuolo, S. Moccia, G. L.Russo, Anti-inflammatory effects of flavonoids in neurodegenerative disorders, Eur J Med Chem, 153 (2018) 105-115.

[29] P.B. Anning, B. Coles, J. Morton, H. Wang, J. Uddin, J.D. Morrow, S.K. Dey, L.J. Marnett, V.B. O'Donnell, Nitric oxide deficiency promotes vascular side effects of cyclooxygenase inhibitors, Blood, 108 (2006) 4059-4062.

[30] F.A. Facchini, L. Zaffaroni, A. Minotti, S. Rapisarda, V. Calabrese, M. Forcella, P. Fusi, C. Airoldi, C. Ciaramelli, J.M. Billod, A.B. Schromm, H. Braun, C. Palmer, R. Beyaert, F. Lapenta, R. Jerala, G. Pirianov, S. Martin-Santamaria, F. Peri, Structure-Activity Relationship in Monosaccharide-Based Toll-Like Receptor 4 (TLR4) Antagonists, J. Med. Chem., 61 (2018) 2895-2909.

[31] H.Z. Yang, J.P. Wang, S. Mi, H.Z. Liu, B. Cui, H.M. Yan, J. Yan, Z. Li, H. Liu, F. Hua, W. Lu, Z.W. Hu, TLR4 activity is required in the resolution of pulmonary inflammation and fibrosis after acute and chronic lung injury, Am J Pathol, 180 (2012) 275-292.

[32] M.T. Ganter, J. Roux, B. Miyazawa, M. Howard, J.A. Frank, G. Su, D. Sheppard, S.M. Violette, P.H. Weinreb, G.S. Horan, M.A. Matthay, J.F. Pittet, Interleukin-1beta causes acute lung injury via alphavbeta5 and alphavbeta6 integrin-dependent mechanisms, Circ Res, 102 (2008) 804-812.

[33] J. Grommes, O. Soehnlein, Contribution of neutrophils to acute lung injury, Mol Med, 17 (2011) 293-307.

[34] B.V. Patel, M.R. Wilson, K.P. O'Dea, M. Takata, TNF-induced death signaling triggers alveolar epithelial dysfunction in acute lung injury, Journal of immunology, 190 (2013) 4274-4282.

[35] L.Z. Chen, W.W. Sun, L. Bo, J.Q. Wang, C. Xiu, W.J. Tang, J.B. Shi, H.P. Zhou, X.H. Liu, New arylpyrazoline-coumarins: Synthesis and anti-inflammatory activity, Eur J Med Chem, 138 (2017) 170-181.

[36] L. Trifonov, V. Nudelman, M. Zhenin, E. Matsree, M. Afri, B. Schmerling, G. Cohen, K. Jozwiak, M. Weitman, E. Korshin, H. Senderowitz, A. Shainberg, E. Hochhauser, A. Gruzman, Structurally Simple, Readily Available Peptidomimetic 1-Benzyl-5-methyl-4-(n-octylamino)pyrimidin-2(1H)-one Exhibited Efficient Cardioprotection in a Myocardial Ischemia (MI) Mouse Model, J. Med. Chem., (2018).

[37] Y. Zhang, Z. Liu, J. Wu, B. Bai, H. Chen, Z. Xiao, L. Chen, Y. Zhao, H. Lum, Y. Wang, H. Zhang, G. Liang, New MD2 inhibitors derived from curcumin with improved anti-inflammatory activity, Eur J Med Chem, 148 (2018) 291-305.

[38] J. B. Shi, L. Z. Chen, B. S. Wang, X. Huang, M. M. Jiao, M. M. Liu, W. J. Tang, X. H. Liu, Novel Pyrazolo[4,3-d]pyrimidine as Potent and Orally Active Inducible Nitric Oxide

Synthase (iNOS) Dimerization Inhibitor with Efficacy in Rheumatoid Arthritis Mouse Model, J Med Chem, 2019, DOI: 10.1021/acs.jmedchem.9b00039.

[39] G. M. Sheldrick, SHELXTL-97, Program for Crystal Structure Solution and Refinement; University of Göttingen: Göttingen, Germany, 1997.

Figure Captions

Figure 1. The continuous workflow

Figure 2. ORTEP drawing of compounds **5r** and **5u**

Figure 3. Inhibition of NO production by all compounds **5a**~**5v** and **7a**~**7o**

Figure 4. The cytotoxic evaluation in RAW264.7 of compounds **5a**~**5v** and **7a**~**7o**

Figure 5. Inhibition of the Cytokine Production production

Figure 6. Compound **7f** inhibited LPS-induced iNOS and COX-2 expression

Figure 7. Compound **7f** inhibits LPS-induced ERK and P38 signaling

Figure 8. Compound **7f** inhibited LPS-induced activation of NF-κB signaling Pathway

Figure 9. The interaction of compound **7f** with TAK1 (PDB ID: 5V5N)

Figure 10. Compound **7f** protected LPS-induced acute lung injury

Figure 11. Effects of compound **7f** on histopathological changes in lung tissues

Figure 12. Prelimilary mechanisms involved

Scheme 1. Synthesis of compounds **3a~3d**

Scheme 2. Synthesis of compounds **5a~5v**

Chemical structures and yields of compounds **5a**~**5v** (**Table 1**)

Scheme 3. Synthesis of compounds **7a~7o**

Chemical structures and yields of compounds **7a~7o** (**Table 2**)

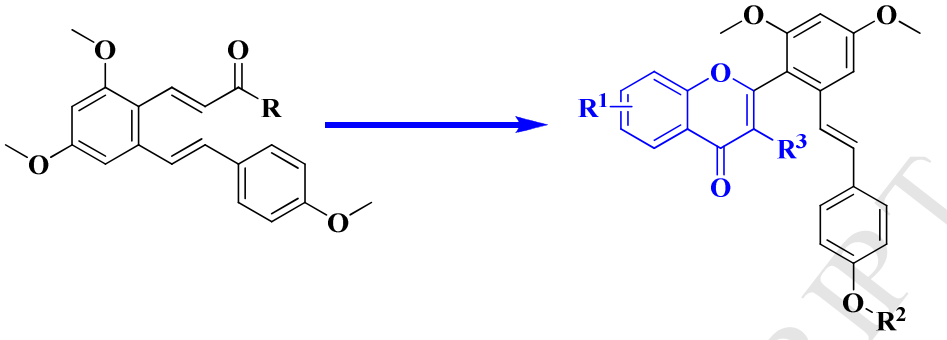

Previous work **This work**

Figure 1. The continuous workflow

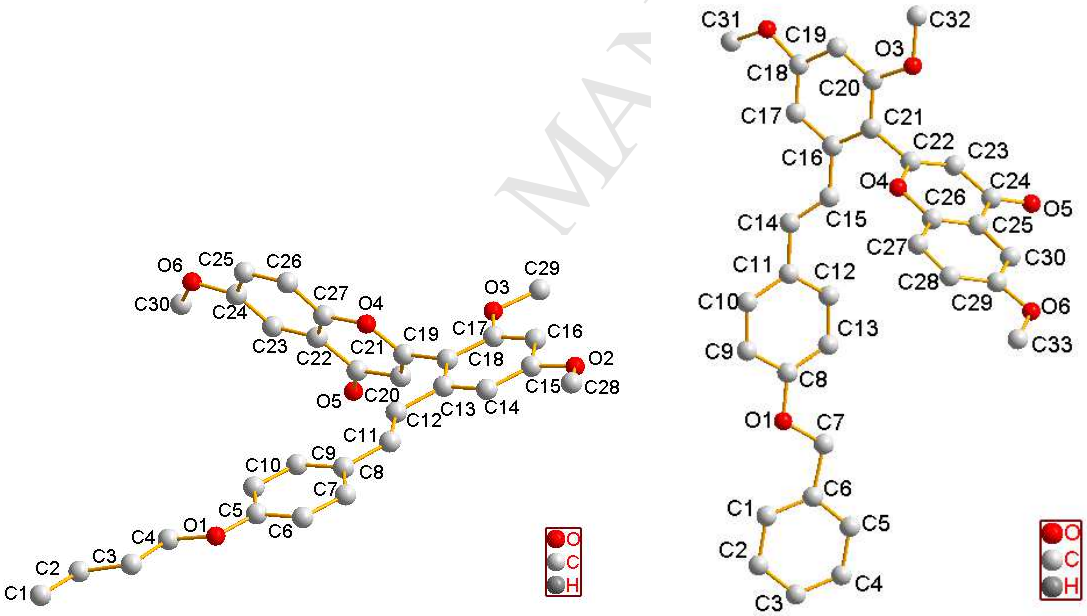

Compound **5r** Compound **5u**

Figure 2. ORTEP drawing of compounds **5r** and **5u**

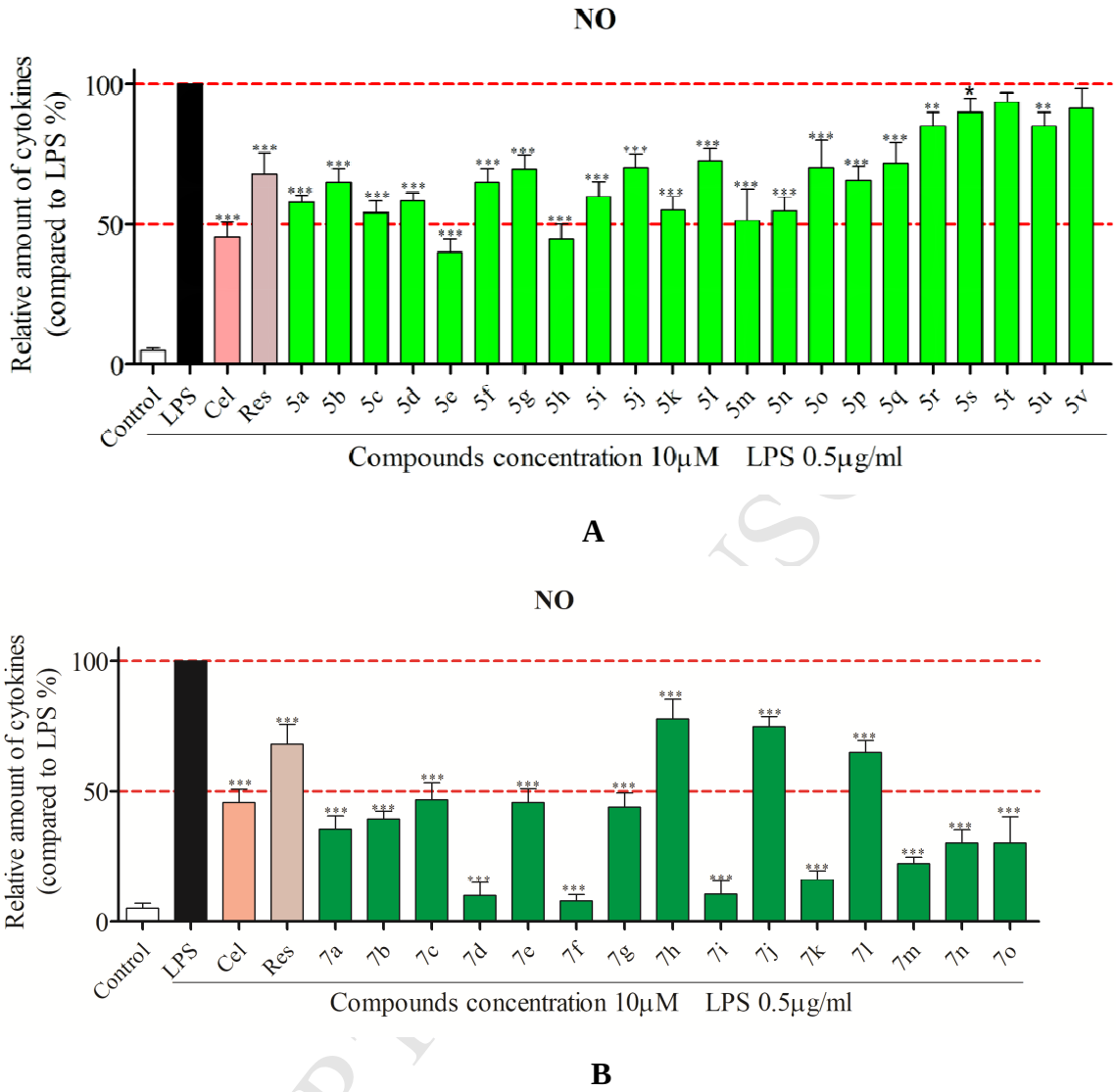

Figure 3. Inhibition of NO production by all compounds **5a**~**5v** and **7a**~**7o** [a]

[a] RAW264.7 cells were pretreated with compounds **5a**~**5v** and **7a**~**7o** (10 μM) for 1 h, incubated with LPS (0.5 μg/mL) for 24 h, NO production was measured using Griess Reagent assay. (**A**) Effects of compounds **5a**~**5v** on NO secretion. (**B**) Effects of compounds **7a**~**7o** on NO secretion. **Cel**: positive compound celecoxib. **Res**: positive compound resveratrol. ***p<0.001, **p<0.01, *p<0.05 *vs* LPS group.

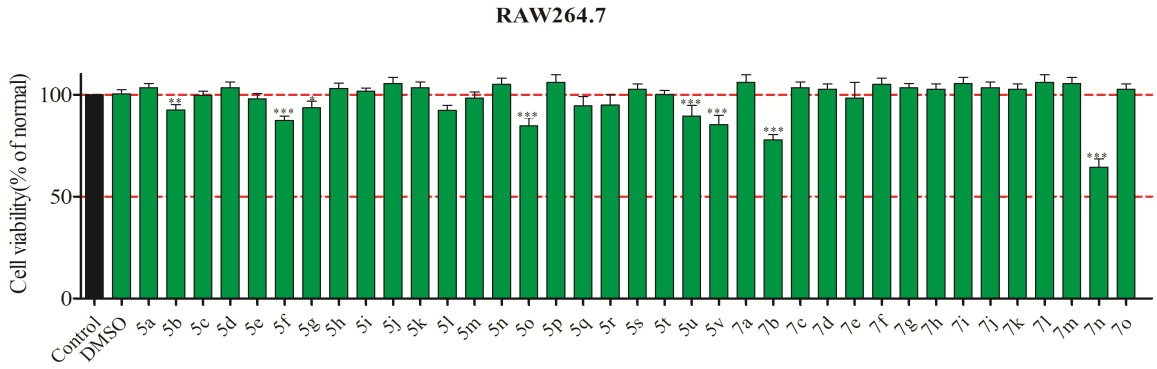

Figure 4. The cytotoxic evaluation in RAW264.7 cells [a]

[a] The cell viability was evaluated by the MTT assay. ***p<0.001 compare with the control group.

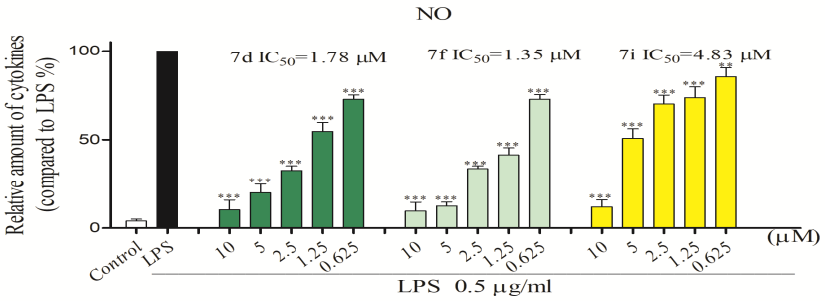

A

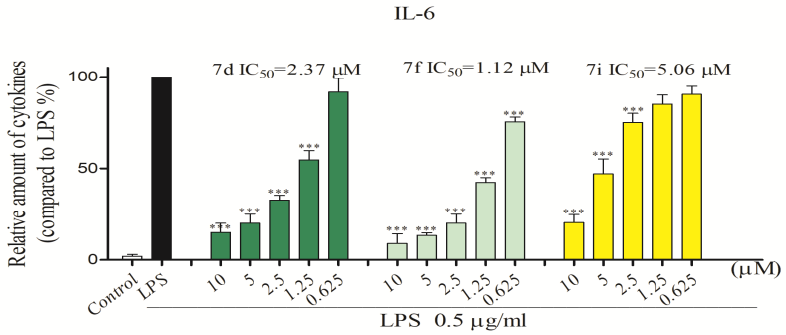

B

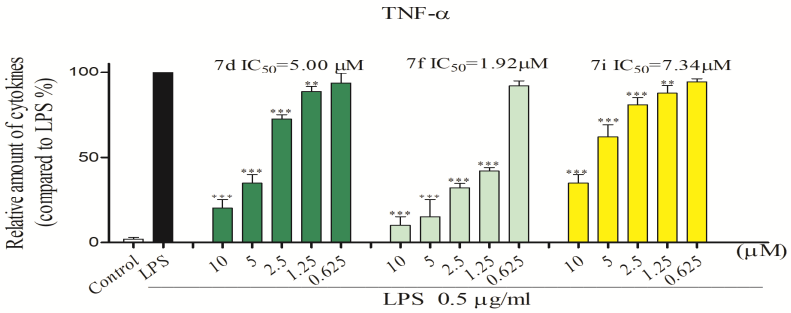

C

Figure 5. Inhibition of the cytokine production [a]

[a] RAW264.7 cells were pretreated with compounds **7d**, **7f** and **7i**, at concentrations of 10, 5, 2.5, 1.25, 0.625 μM for 1 h, incubated with LPS (0.5 μg/mL) for 24 h, NO production was measured using Griess Reagent assay. The levels of TNF-α and IL-6 in the culture medium were measured by ELISA. ***p<0.001, **p<0.01, *p<0.05 *vs* LPS group.

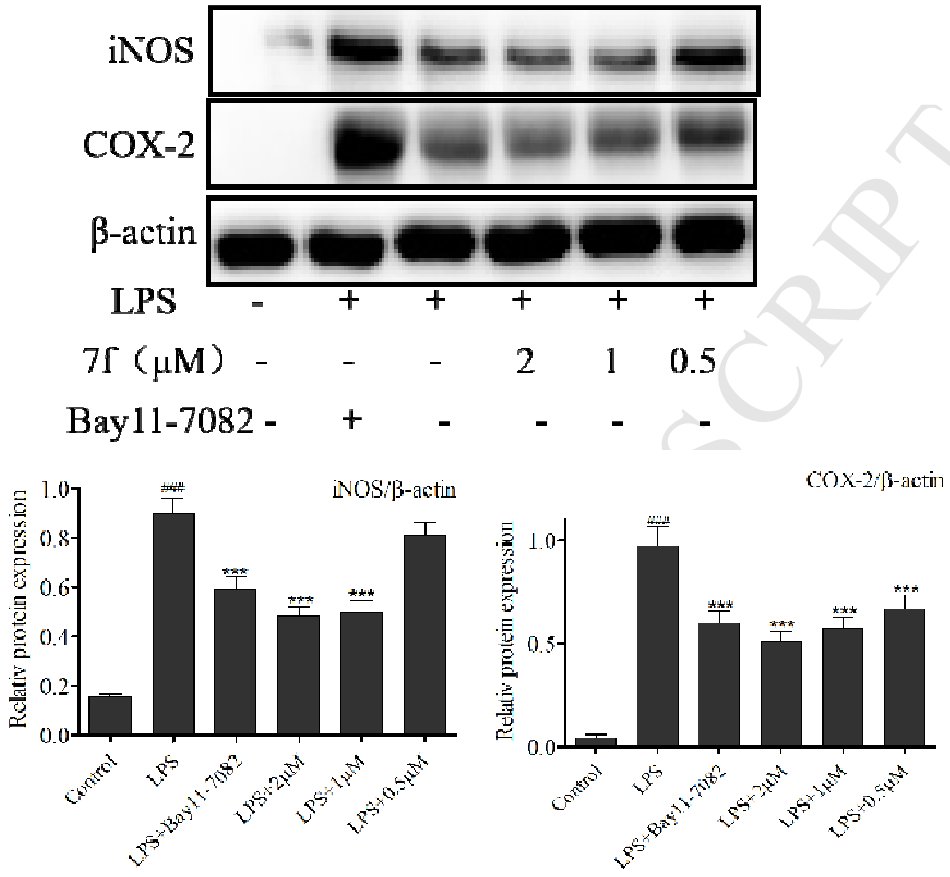

Figure 6. Compound **7f** inhibited expression LPS-induced iNOS and COX-2 [a]

[a]After pretreatment with compound **7f** (0.5~2 μM) 1 h, RAW 264.7 cells were stimulated with LPS (0.5 μg/mL) for 24 h. iNOS, COX-2 and β-actin were detected by Western blot. Bay11-7082 used as the NF-κB inhibitor. $^{###}p<0.001$ compared with LPS unstimulated cells, $^{***}p<0.001$, $^{**}p<0.01$, $^{*}p<0.05$ compared with LPS-stimulated cells; The blots shown are the examples of three separate experiments.

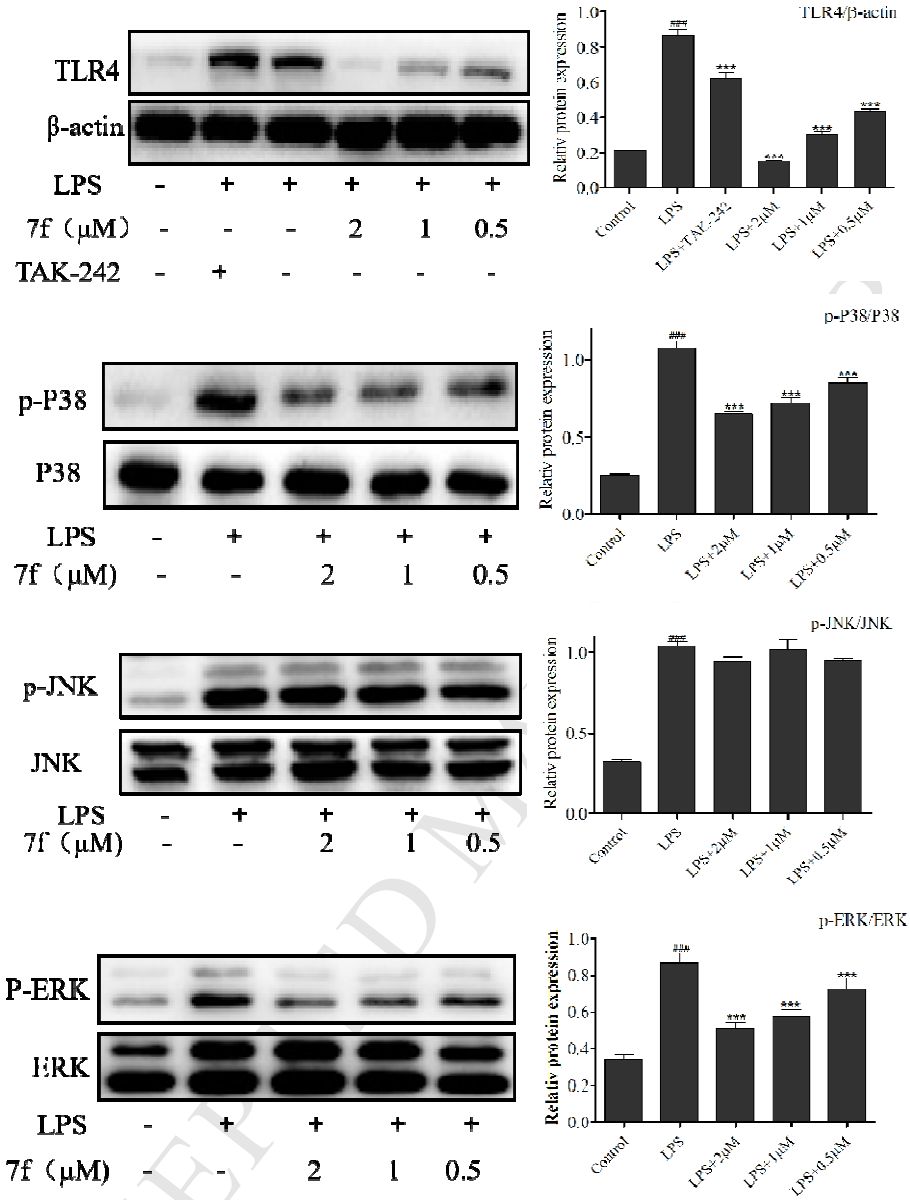

Figure 7. Compound **7f** inhibited LPS-induced ERK and P38 signaling [a]

[a] Compound **7f** time-dependently suppressed LPS-induced P38 and ERK activation. RAW264.7 cells were pre-treated with compound **7f** (0.5~2 μM) for 1 h, then stimulated with LPS (0.5 μg/mL) for 30 min, the expression of phosphor and total proteins ERK, JNK, and p38 were analyzed by Western blot. TAK-242 used as the TLR4 inhibitor. The results were showed as means ± SD (n=3) of at least three independent experiments. $^{###}p<0.001$ $^{*}p<0.05$, $^{**}p<0.01$, $^{***}p<0.001$ compare with LPS-stimulated cells.

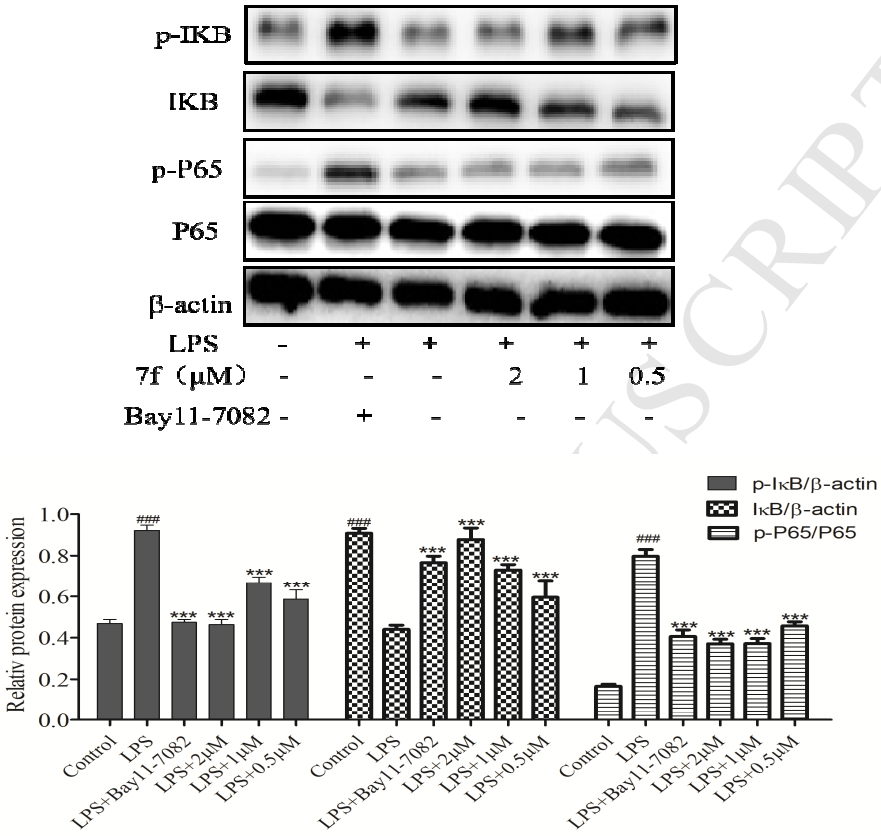

Figure 8. Compound **7f** inhibited LPS-induced activation of NF-κB signaling pathway in RAW 264.7 cells [a]

[a] After pretreatment with compound **7f** (0.5~2 μM) 1 h, RAW 264.7 cells were stimulated with LPS (0.5 μg/mL) for 30 min. P-IKB IKB, p-P65, P65 and β-actin were detected by Western blot. Bay11-7082 used as the NF-κB inhibitor. $^{###}p<0.001$ compared with LPS unstimulated cells, $^{***}p<0.001$, $^{**}p<0.01$, $^{*}p<0.05$ compared with LPS-stimulated cells; The blots shown are the examples of three separate experiments.

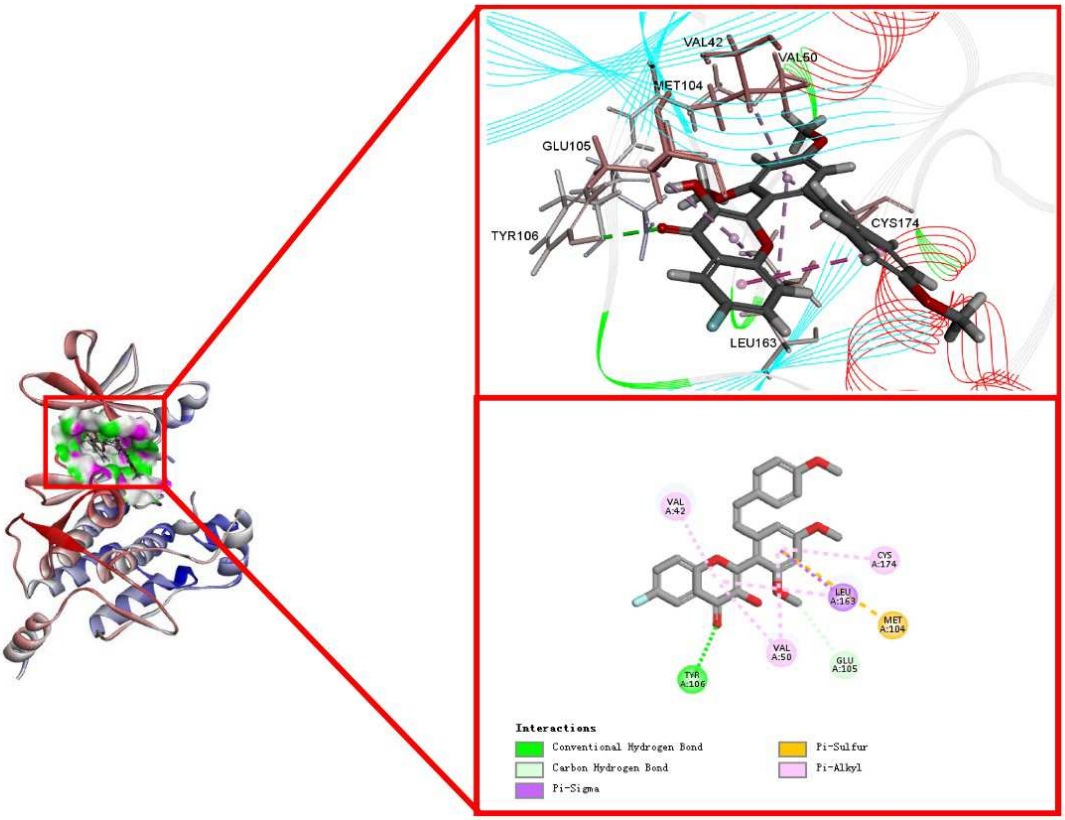

Figure 9. The interaction of compound **7f** with TAK1 (PDB ID: 5V5N)

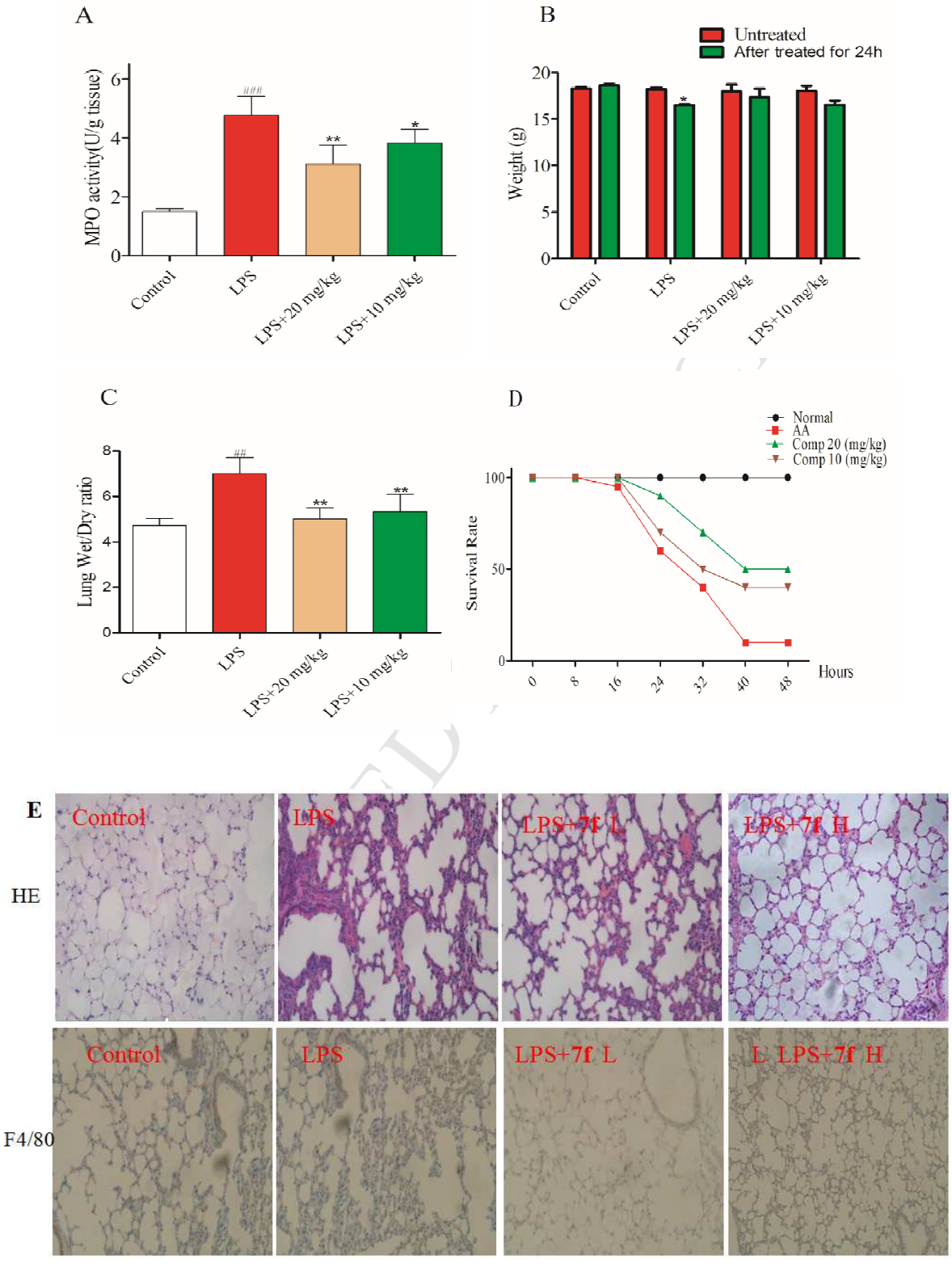

Figure 10. Compound **7f** protected LPS-induced acute lung injury [a]

[a] C57/BL6 mice were treated by intraperitoneal injection with compound **7f** (10 mg/kg, 20 mg/kg), and after 30 min, were challenged with 5 mg/kg LPS by intratracheal injection. (**A**) Myeloperoxidase (MPO) activity of lung tissue. (**B**) Body weight changes. (**C**) Pulmonary Edema: lung wet/dry ratio. (**D**) Survival of miance in a model. (**E**) Effects of compound **7f** on histopathological changes in lung tissues by LPS (H&E staining and immunohistochemical of F4/80 staining 200×).

$^{###}p<0.001$ compared with control group; $^{*}p<0.05$, $^{**}p<0.01$, $^{***}p<0.001$ compare with LPS group.

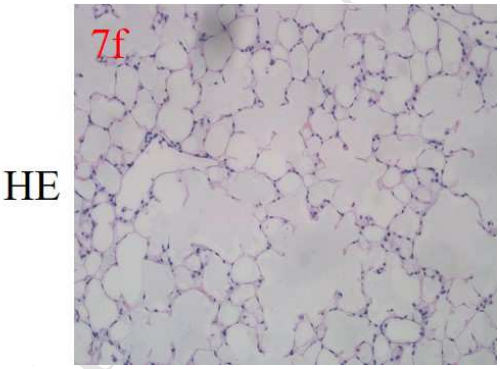

Figure 11. Effects of compound **7f** on histopathological changes in lung tissues

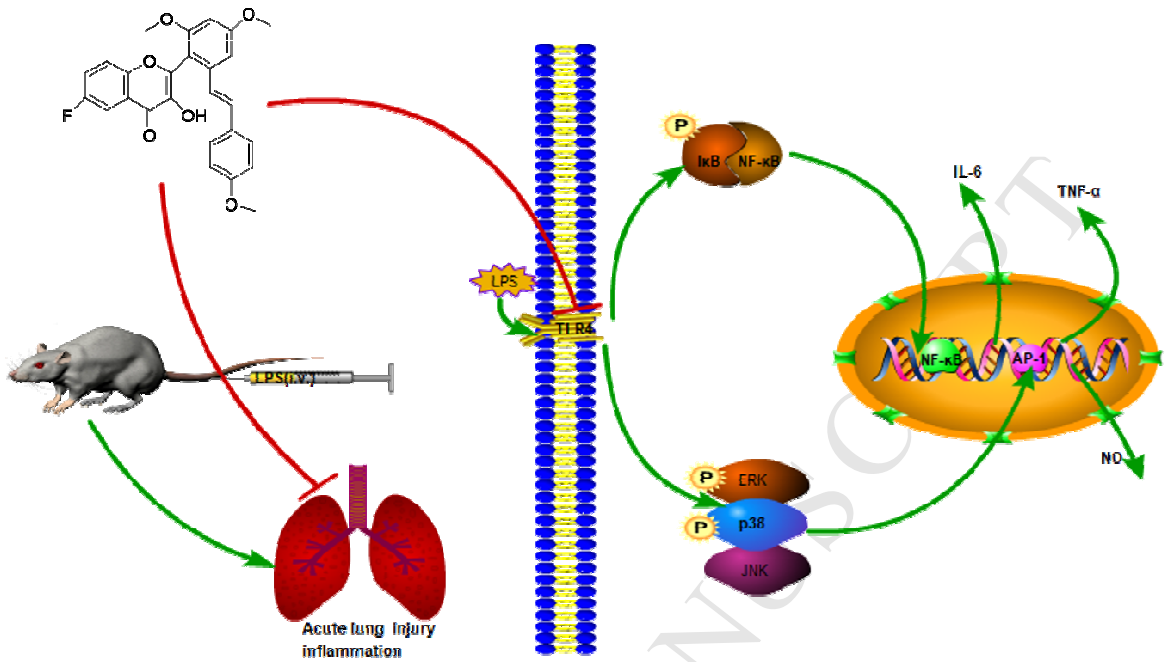

Figure 12. Prelimilary mechanisms involved

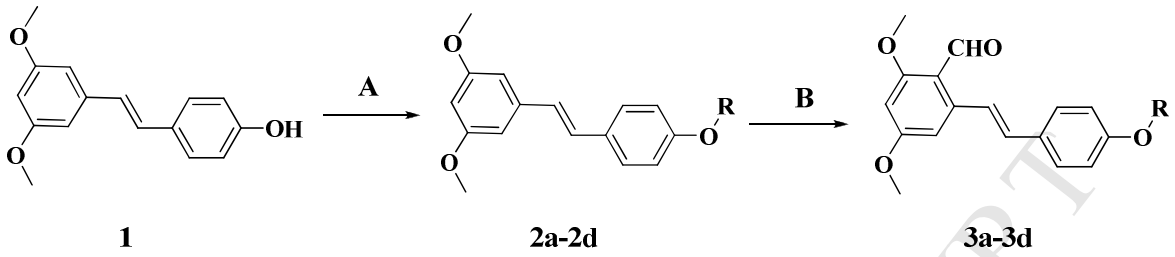

Scheme 1. Synthesis of compounds **3a~3d**

Reagents and conditions: (**A**) TBAB, K_2CO_3, Acetone, reflux, 3-6 h; (**B**) DMF, $POCl_3$, Acetonitrile, 0 °C, rt, 1.5 h.

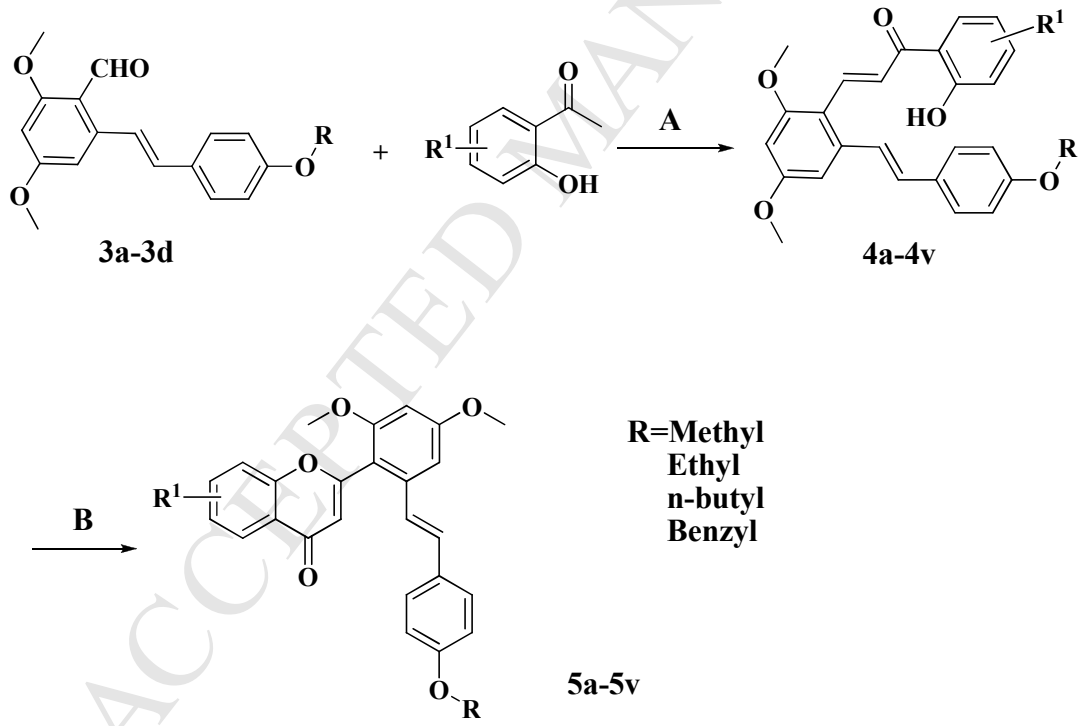

Scheme 2. Synthesis of compounds **5a~5v**

Reagents and conditions: (**A**) Pyrolidine, Ethanol, 40°C, 36 h; (**B**) I_2, DMSO, reflux, 4-6 h.

Table 1. Chemical structures and yields of compounds **5a**~**5v**

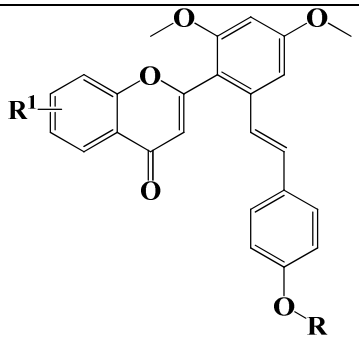

Comp.	**R**	**R^1**	Yield (%)	Comp.	**R**	**R^1**	Yield (%)
5a	Me	H	90	**5l**	Me	4-Br	75
5b	Me	4-CH_3	61	**5m**	Me	5-Br	88
5c	Me	5-CH_3	59	**5n**	Et	H	93
5d	Me	4,5-CH_3	72	**5o**	Et	5-OCH_3	83
5e	Me	5-OCH_3	66	**5p**	Et	5-Br	88
5f	Me	4,5-OCH_3	42	**5q**	n-butyl	H	89
5g	Me	4-F	78	**5r**	n-butyl	5-OCH_3	78
5h	Me	5-F	59	**5s**	n-butyl	5-Br	79
5i	Me	3-Cl	58	**5t**	Benzyl	H	92
5j	Me	4-Cl	68	**5u**	Benzyl	5- OCH_3	76
5k	Me	5-Cl	71	**5v**	Benzyl	5-Br	78

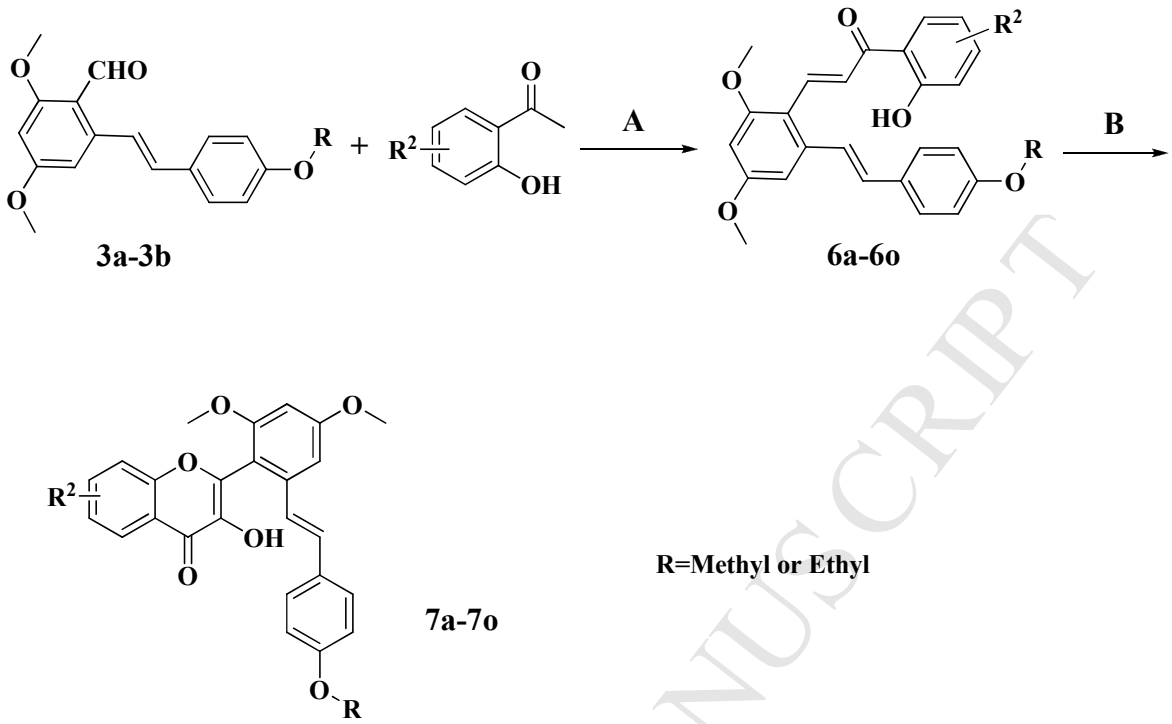

Scheme 3. Synthesis of compounds **7a~7o**

Reagents and conditions: (a) Pyrolidine, Ethanol, 40°C, 36 h; (b) NaOH, 30% H_2O_2, Methanol, 40 °C, 48 h.

Table 2. Chemical structures and yields of compounds **7a**~**7o**

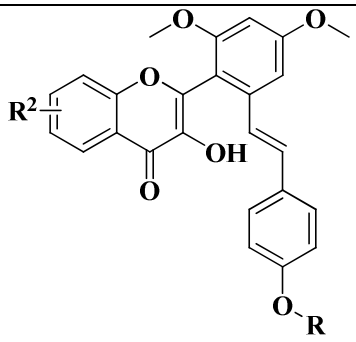

Comp.	**R**	**R^2**	Yield (%)	Comp.	**R**	**R^2**	Yield (%)
7a	Me	H	76	**7i**	Me	5-Cl	60
7b	Me	4-CH_3	78	**7j**	Me	4-Br	76
7c	Me	5-CH_3	44	**7k**	Me	5-Br	82
7d	Me	5-OCH_3	89	**7l**	Me	4,5-CH_3	66
7e	Me	4-F	63	**7m**	Et	H	77
7f	Me	5-F	68	**7n**	Et	5-OCH_3	81
7g	Me	3-Cl	55	**7o**	Et	5-Br	78
7h	Me	4-Cl	48				

Highlights

► Novel resveratrol-based flavonol compounds were synthesized.

► Compound showed high anti-inflammatory activity against IL-6、NO and TNF-α.

► Preliminary mechanisms of anti-inflammatory action were discovered.